Copy
RM L9L09

RESEARCH MEMORANDUM

THE EFFECT OF CHANGES IN THE LEADING-EDGE RADIUS ON THE AERODYNAMIC CHARACTERISTICS OF A SYMMETRICAL, 9-PERCENT-THICK AIRFOIL AT HIGH-SUBSONIC MACH NUMBERS

By Milton D. Humphreys and Raymond A. Robinson

Langley Aeronautical Laboratory
Langley Air Force Base, Va.

NATIONAL ADVISORY COMMITTEE
FOR AERONAUTICS

WASHINGTON

August 7, 1950

NATIONAL ADVISORY COMMITTEE FOR AERONAUTICS

RESEARCH MEMORANDUM

THE EFFECT OF CHANGES IN THE LEADING-EDGE RADIUS ON THE AERODYNAMIC CHARACTERISTICS OF A SYMMETRICAL, 9-PERCENT-THICK AIRFOIL AT HIGH-SUBSONIC MACH NUMBERS

By Milton D. Humphreys and Raymond A. Robinson

SUMMARY

To investigate in more detail the effect of leading-edge radius on the high-speed aerodynamic characteristics of a symmetrical, 9-percent-thick airfoil, tests were made of the NACA 0009-64, 0009-54, and 0009-44 airfoils. These airfoils have leading-edge radii of 0.893, 0.620, and 0.397 percent of the chord, respectively. The tests were conducted in the Langley rectangular high-speed tunnel at Mach numbers from approximately 0.30 to the choking value ($M = 0.89$ at $\alpha = 0^\circ$) for angles of attack from 0° to 8°. The Reynolds number range corresponding to the Mach number range of this investigation was from 0.7×10^6 to 1.5×10^6.

This investigation showed that for Mach numbers up to 0.825 the leading-edge radius of these airfoils does not greatly influence either the section normal-force, drag, and pitching-moment coefficients or the Mach number of normal-force break. At a Mach number of 0.850 the drag of the NACA 0009-54 airfoil appeared to be 12 to 25 percent lower than that of the other airfoils for normal-force coefficients in the range 0 to 0.3.

INTRODUCTION

An early investigation (reference 1) showed the effect of large changes of leading-edge radius on the high-speed aerodynamic characteristics of 9-percent-thick airfoils. (The changes in the leading-edge radius were accompanied by corresponding systematic changes in the airfoil ordinates from the leading edge back to the position of

maximum thickness (reference 1).) From these tests it was concluded that the optimum value of leading-edge radius was between 0.220 and 0.893 percent of the chord.

The purpose of the present investigation was to determine the effects of changes of leading-edge radius within this range on the high-speed aerodynamic characteristics of symmetrical 9-percent-thick airfoils having their maximum thickness located at the 40-percent-chord station. To obtain this information, the NACA 0009-64, 0009-54, and 0009-44 airfoils were tested in the Langley rectangular high-speed tunnel. Normal-force, drag, and pitching-moment coefficients were determined from static-pressure measurements along the airfoil surfaces and total-pressure measurements in the model wakes. Pressure measurements were made at Mach numbers from approximately 0.30 to the choking value ($M = 0.89$ at $\alpha = 0^\circ$) for the tunnel, for angles of attack from 0° to 8°. Schlieren photographs were also taken.

The results of a concurrent investigation of leading-edge-radius effects (reference 2) are summarized and compared with the present results in the discussion.

SYMBOLS

c_d	section drag coefficient
$c_{m_{c/4}}$	section pitching-moment coefficient of normal force about quarter-chord location
c_n	section normal-force coefficient
M	stream Mach number
M_{cr}	critical Mach number
p	stream static pressure
p_l	local static pressure
q	stream dynamic pressure
P	pressure coefficient $\left(\frac{p_l - p}{q}\right)$
P_{cr}	critical pressure coefficient corresponding to local Mach number = 1.0
α	angle of attack

[redacted]

APPARATUS, MODELS, AND TESTS

The 4-inch-chord airfoils were tested in the Langley rectangular high-speed tunnel (reference 3), which has a 4- by 18-inch test section. The models spanned the 4-inch dimension of the test section.

The airfoils investigated are designated according to the system used in reference 1 as:

NACA 0009-64

NACA 0009-54

NACA 0009-44

The leading-edge-radius index is given by the first digit after the dash. The corresponding radii in percent of chord for the 9-percent-thick models are as follows:

Index	Leading-edge radius (percent chord)
6	0.893
5	.620
4	.397

The other digits in order indicate the camber, zero; position of maximum camber, zero; thickness, 9 percent; and location of maximum thickness, 40 percent of the chord.

Changing the leading-edge radius resulted in systematic changes in the airfoil profiles to the 40-percent-chord station. Figure 1 shows the ordinates to an enlarged scale and figure 2 shows the ordinates and orifice locations to actual scale. The ordinates are tabulated in table I.

The tests consisted of making static-pressure measurements along the airfoil surfaces and total-pressure measurements in the wakes. These measurements were made at Mach numbers from approximately 0.30 to the choking value for the tunnel ($M = 0.89$ at $\alpha = 0^\circ$), for angles of attack from 0° to 8°. Reynolds numbers, corresponding to these speeds, varied from approximately 0.7×10^6 to 1.5×10^6. To supplement the tests, schlieren photographs were taken at Mach numbers comparable to those obtained in the pressure-distribution tests, for angles of attack from 0° to 6°.

[redacted]

CORRECTIONS AND PRECISION

The data, except for the pressure coefficients, have been corrected for constriction effects. These corrections, which were computed by the method of reference 4, were applied to the normal-force coefficients, drag coefficients, pitching-moment coefficients, and Mach number. Although the Mach numbers of the pressure distributions presented have been corrected, the pressure coefficients themselves have not been corrected, primarily because they are presented for illustrative and comparative purposes only.

Since there is no method of correcting for the flow distortions at and near choking, the data from 0.03 below choking to the choking Mach number are either shown as dashed lines on the figures, or not shown at all.

The accuracy of the initial alinement of the model with the air stream is of the order of 0.2° at the 0° angle-of-attack setting. All incremental angle-of-attack settings measured from the initial zero setting were accurate to $\pm 0.05^\circ$ of the angles indicated. The test points at 2° angle of attack in figure 3(a) indicate the precision of the data.

RESULTS

The variation of the section normal-force coefficients with Mach number for each of the three airfoils is given in figure 3. Figure 4 presents a direct comparison between the normal-force coefficients obtained at constant angles of attack from 0° to 8° over the Mach number range for the airfoils. Figure 5 shows the variation of normal-force coefficient with angle of attack and the variation of moment coefficient with normal-force coefficient for each airfoil at several Mach numbers. Figure 6 presents a comparison of the normal-force curves for the three airfoils at high Mach numbers. The drag coefficients for 0°, 2°, 4°, and 6° angles of attack (fig. 7) were obtained from wake-survey measurements. At 8° the drag coefficients were determined from the airfoil pressure distributions. To take into account the viscous drag effects for the 8° condition, 0.006 has been added to the pressure-drag-coefficient measurements. The drag polars for the airfoils (fig. 8) are cross plots of figures 3 and 7. Figure 9 is a direct comparison of the drag polars for the three airfoils at high Mach numbers. The variation of moment coefficient with Mach number is presented in figure 10. Figures 11 and 12 show the pressure distributions for these sections. To illustrate the flow, several schlieren photographs are also given (fig. 13). Figure 14 presents a comparison of the results with data obtained in other tunnels.

[redacted]

DISCUSSION

Normal-force coefficients.- The Mach number for normal-force break is defined as the Mach number at which the rate of change of normal force with Mach number is zero or slightly negative for constant angle of attack. Figures 3 and 4, especially 4, indicate that changing the leading-edge radius from 0.397 to 0.893 percent chord on the 9-percent-thick airfoils investigated produced only small differences in the Mach number for normal-force break for all the airfoils investigated. For example, at 2° angle of attack (fig. 4), although changes in leading-edge radius had an appreciable effect on the critical Mach number, the effect on the Mach number of normal-force break was negligibly small.

In general, the normal-force-curve slopes for all the airfoils at constant normal-force coefficients below 0.30 increase with Mach number up to near 0.825, with the NACA 0009-64 airfoil having the highest slope and the NACA 0009-44 airfoil having the lowest slope at this Mach number (figs. 5 and 6). At a Mach number of 0.85, the leading-edge radius of 0.620 percent chord of the NACA 0009-54 airfoil produced a higher normal-force-curve slope for normal-force coefficients from 0 to 0.3 than did the larger or smaller leading-edge radius of the other two airfoils.

Drag coefficients.- As with the normal-force characteristics, the drag characteristics do not differ greatly for the three airfoils up to a Mach number of 0.825 (figs. 7 and 8). At a Mach number of 0.850 a comparison of the drag polars for the airfoils (fig. 9) indicates that the NACA 0009-54 airfoil has drag coefficients 12 to 25 percent lower than for the other two airfoils at normal-force coefficients from 0 to 0.3. A part of this apparent improvement in the drag characteristics shown for the NACA 0009-54 airfoil is attributed to the higher lift-curve slope for the airfoil at this Mach number (fig. 6).

Moment coefficients about the quarter chord.- The change in moment coefficient with Mach number for constant normal-force coefficients up to 0.30 (fig. 5) is smallest for the NACA 0009-44 airfoil, while the moment coefficient for the NACA 0009-64 airfoil showed the widest variation with Mach number of the three airfoils tested. For a constant angle of attack of 2°, figure 10 showed the NACA 0009-44 airfoil to have the smallest and the NACA 0009-64 airfoil the largest variation of moment coefficient with Mach number. The wider variation in moment coefficient with increases in Mach number from 0.80 to 0.85 for the NACA 0009-64 airfoil was caused by a larger reduction in load over the forward portion, and a more rearward movement of the loading on this airfoil than for the

other airfoils for normal-force coefficients up to 0.3 (fig. 12(b)). At normal-force coefficients greater than 0.30 the variation of moment coefficient with Mach number for constant normal-force coefficients did not differ greatly for the three airfoils (fig. 5).

Pressure-distribution diagrams.- Experimental pressure distributions obtained at low Mach numbers on the airfoils at 0° angle of attack were extrapolated to zero Mach number using the Prandtl-Glauert relation. (The experimental pressure distributions at 0° used in the extrapolation are the average values for the upper and lower surfaces.) The theoretical pressure distributions were obtained by the methods of references 5 and 6 as outlined in reference 7. A comparison of the extrapolated pressure distributions at zero Mach number with the theoretical distributions for incompressible flow shows excellent agreement (fig. 11). Figure 11 shows the effect of changing the leading-edge radius on the pressure distributions for these airfoils at low speeds. The effect is particularly marked over the forward half of the airfoil and shows up in the maximum induced velocity attained and in the accelerations near the leading edge. A reduction in the leading-edge radius decreased the accelerations over the leading edge and decreased the maximum induced velocity that occurred on the airfoil. This is illustrated by a comparison of the pressure distributions for the NACA 0009-64 and NACA 0009-44 airfoils.

From considerations of velocity correction factors, such as the Prandtl-Glauert relation, these differences might be expected to increase with increasing Mach number; consequently, their high-speed section characteristics at low angles of attack might be expected to differ appreciably. The test results, however, have shown that the differences in forces and moments are small at Mach numbers less than 0.80. The reason that the measured differences in aerodynamic characteristics were small is shown by the experimental pressure distributions (fig. 12). For $\alpha = 0°$ and $M = 0.30$ (fig. 12(a)) the pressure distributions differ as predicted by theory. With increasing Mach number, instead of obtaining the differences between the pressure distributions predicted by the correction theory, the pressures at the 40-percent-chord station decreased more rapidly than those close to the nose, so that at Mach numbers between 0.80 and 0.84 the minimum pressure for each airfoil at 0° angle of attack occurs near the 40-percent-chord station.

For all angles of attack the pressure distributions shown in figure 12 indicate that the small differences in the low-speed pressure distributions were (in general) diminished, rather than magnified, as the Mach number was increased up to a Mach number of 0.80. Therefore the aerodynamic characteristics of these airfoils were not greatly influenced by the changes in leading-edge radius investigated over this Mach number range.

[redacted]

Schlieren photographs.- The schlieren photographs (fig. 13) indicate the general similarity of the supercritical flow characteristics about the three airfoils. The flow having exceeded the local velocity of sound exhibits shock waves, indicated by the light vertical lines in the pictures. The weak disturbances (fig. 13(a)) at subcritical speeds ($M = 0.76$) should not be confused with true shock waves. They are weak flow disturbances which have been previously observed at subcritical Mach numbers (reference 8) and are picked up by the highly sensitive schlieren system used in this investigation. Separation effects and flow turbulence are indicated by the dark horizontal lines and eddies appearing in schlieren photographs. In figure 13(a) for the NACA 0009-54 airfoil the light beam appears to be slightly misalined and shows reflections over the rear upper surface resembling a thick boundary layer. The reflections should be discounted in comparing the three airfoils in figure 13(a).

Comparison of the results with data obtained in other tunnels.- The results of a concurrent investigation of the effects of leading-edge radius have recently been published in reference 2. Of the airfoils reported, the NACA 0010-1.10 40/1.575, 0010-0.70 40/1.575, and the 0010-0.27 40/1.575 airfoils correspond to the NACA 0010-64, 0010-54, and 0010-34 airfoils (using the customary NACA airfoil designations of references 1 and 7). These airfoils can be compared with the similar 9-percent-thick airfoils in the present paper. The remaining airfoils of reference 2 are not directly comparable to those reported herein because of differences in their design parameters affecting the airfoil surface curvature and consequently the pressure distributions. (Compare with reference 1.)

The data for the NACA 0010-64 and 0010-54 airfoils in reference 2 are in agreement with data of the corresponding 9-percent-thick airfoils of the present paper in indicating no appreciable effect of leading-edge radius on the normal-force-curve slope at Mach numbers below 0.775. In this lower Mach number range, references 1 and 2 both showed that the NACA 0010-34 airfoil had the highest normal-force-curve slope. (See fig. 14(b).) At the higher Mach numbers, the results of the present investigation as well as references 1 and 2 show that a large decrease in leading-edge radius produces an appreciable decrease in the normal-force-curve slope. The effects of a small reduction in leading-edge radius from the normal leading-edge radius (NACA 0009-64 airfoil) are shown by the results of the present investigation and reference 2. The two investigations are in large disagreement in that the present investigation shows a small favorable increase, whereas reference 2 shows a very large unfavorable decrease in normal-force-curve slope with a small decrease in leading-edge radius. A large change in normal-force-curve slope with small change in leading-edge radius would not have been expected, although no reason can be found for the diversity of effects

[redacted]

shown by the two investigations. The accuracy of the profiles in the present investigation is verified by the close agreement of the experimental and theoretical pressure distributions in figure 11.

The drag data of the comparable airfoils of the present report and references 1 and 2 were in agreement in indicating that the minimum section drag coefficient was not significantly influenced by leading-edge-radius variations for Mach numbers up to 0.75. At Mach numbers near 0.85 and normal-force coefficients of 0 and 0.2, it is significant that large reductions in the leading-edge radius produced an increase in the section drag coefficients for the airfoils reported in references 1 and 2 and the present paper. The airfoils having the smallest leading-edge radii produced the highest drag in each case. Again there is disagreement in the data of the present paper and reference 2 as to the effect of small reductions in the leading-edge radius on the section drag coefficients at Mach numbers above 0.825; the present investigation shows a favorable reduction in drag coefficient, whereas reference 2 shows an increase in drag coefficient with a small decrease in leading-edge radius from the normal value.

The general trend of the pitching-moment data of reference 2, shown as $\frac{dc_m}{dc_n}$ against M in figure 14(a), is in large disagreement with the data of the present paper and with comparable data from other tunnels. (See references 1, 9, and 10, and fig. 14(a).) The aerodynamic center was, in general, located rearward of the quarter-chord location for the airfoils of reference 2 at all Mach numbers. The data of the present paper, in general agreement with available data from several other tunnels (references 1, 9, and 10), indicated that the aerodynamic center was located ahead of the quarter-chord location at low Mach numbers and moved farther forward as the Mach number was increased to values approaching the normal-force break. At higher Mach numbers, there was, in general, a large rearward shift in the aerodynamic center.

CONCLUSIONS

Tests to determine the effect of changes in leading-edge radius on the high-speed aerodynamic characteristics of a 9-percent-thick symmetrical airfoil were made in the Langley rectangular high-speed tunnel at Mach numbers from 0.3 to 0.89, and at corresponding Reynolds numbers from 0.7×10^6 to 1.5×10^6. The results show that within the range of this investigation changes in the leading-edge radii of these airfoils from 0.893 to 0.397 percent chord do not greatly influence

either the section normal-force, drag, and pitching-moment coefficients or the Mach number of normal-force break for Mach numbers up to 0.825. At a Mach number of 0.85 the drag of the NACA 0009-54 airfoil, having a leading-edge radius of 0.620 percent chord, appeared to be 12 to 25 percent lower than that of the other airfoils for normal-force coefficients in the range 0 to 0.3.

Langley Aeronautical Laboratory
National Advisory Committee for Aeronautics
Langley Air Force Base, Va.

[redacted]

REFERENCES

1. Stack, John, and Von Doenhoff, Albert E.: Tests of 16 Related Airfoils at High Speeds. NACA Rep. 492, 1934.

2. Summers, James L., and Graham, Donald J.: Effects of Systematic Changes of Trailing-Edge Angle and Leading-Edge Radius on the Variation with Mach Number of the Aerodynamic Characteristics of a 10-Percent-Chord-Thick NACA Airfoil Section. NACA RM A9G18, 1949.

3. Daley, Bernard N., and Humphreys, Milton D.: Effects of Compressibility on the Flow past Thick Airfoil Sections. NACA TN 1657, 1948.

4. Allen, H. Julian, and Vincenti, Walter G.: The Wall Interference in a Two-Dimensional-Flow Wind Tunnel with Consideration of the Effects of Compressibility. NACA Rep. 782, 1944.

5. Theodorsen, Theodore: Theory of Wing Sections of Arbitrary Shape. NACA Rep. 411, 1931.

6. Naiman, Irven: Numerical Evaluation by Harmonic Analysis of the ϵ-Function of the Theodorsen Arbitrary-Airfoil Potential Theory. NACA ARR L5H18, 1945.

7. Abbott, Ira H., Von Doenhoff, Albert E., and Stivers, Louis S., Jr.: Summary of Airfoil Data. NACA Rep. 824, 1945.

8. Lindsey, W. F., and Daley, Bernard N.: Effects of Compressibility on the Flow past a Two-Dimensional Bump. NACA RM L6K12b, 1947.

9. Polhamus, Edward C.: Preliminary Correlation of the Effect of Compressibility on the Location of the Section Aerodynamic Center At Subcritical Speeds. NACA RM L8D14, 1948.

10. Feldmann, Fritz K.: Untersuchung von symmetrischen Tragflügelprofilen bei hohen Unterschallgeschwindigkeiten in einem geschlossenen Windkanal. Mitt. no. 14, Inst. für Aerod. Tech. H. S. Zürich, Gebr. Leemann & Co. (Zürich), 1948.

[redacted]

[redacted]

TABLE I.- ORDINATES OF AIRFOILS

[Stations and ordinates in percent of wing chord]

NACA 0009-64	
Station	Upper or lower surface ordinate
0	0
1.25	1.360
2.50	1.840
5.00	2.450
7.50	2.860
10.00	3.180
15.00	3.650
20.00	3.970
30.00	4.370
40.00	4.500
50.00	4.370
60.00	3.987
70.00	3.358
80.00	2.493
90.00	1.401
95.00	.770
100.00	.090
L. E. radius: 0.893	

NACA 0009-54	
Station	Upper or lower surface ordinate
0	0
1.25	1.188
2.50	1.646
5.00	2.256
7.50	2.692
10.00	3.035
15.00	3.553
20.00	3.923
30.00	4.364
40.00	4.500
50.00	4.370
60.00	3.987
70.00	3.358
80.00	2.493
90.00	1.401
95.00	.772
100.00	.090
L. E. radius: 0.620	

NACA 0009-44	
Station	Upper or lower surface ordinate
0	0
1.25	1.020
2.50	1.452
5.00	2.062
7.50	2.519
10.00	2.889
15.00	3.461
20.00	3.873
30.00	4.358
40.00	4.500
50.00	4.370
60.00	3.987
70.00	3.358
80.00	2.493
90.00	1.401
95.00	.772
100.00	.090
L. E. radius: 0.397	

[redacted]

NACA

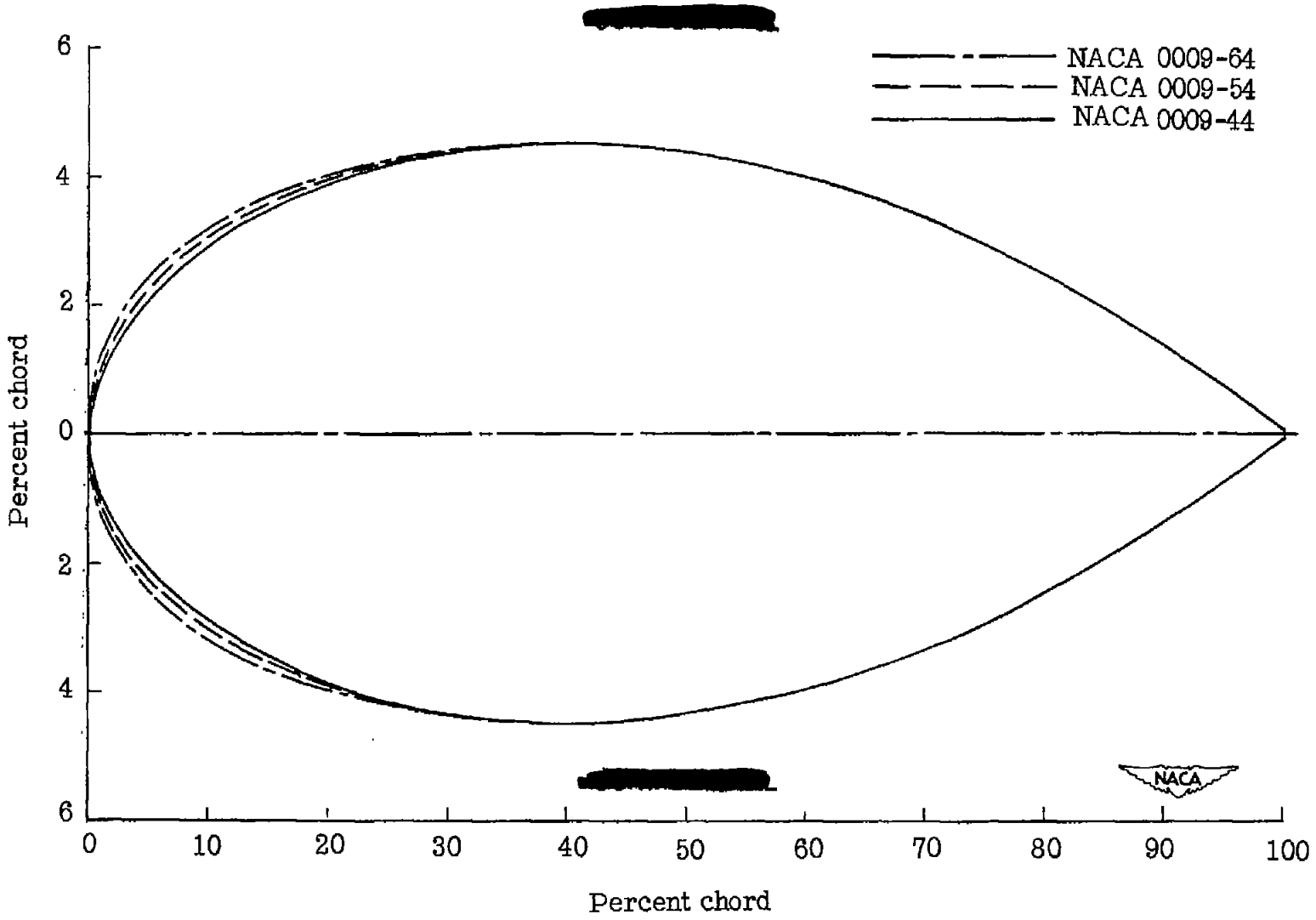

Figure 1.- Comparison of airfoil profiles.

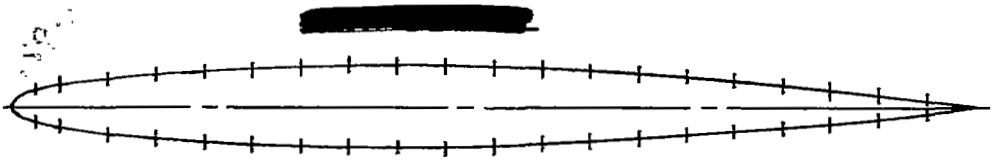

NACA 0009-64

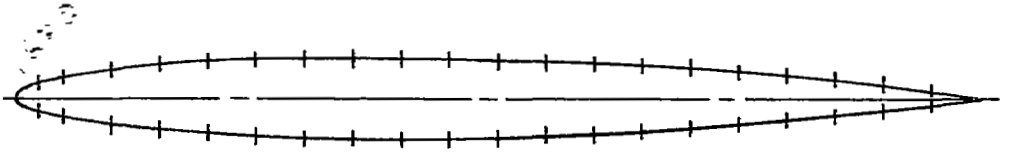

NACA 0009-54

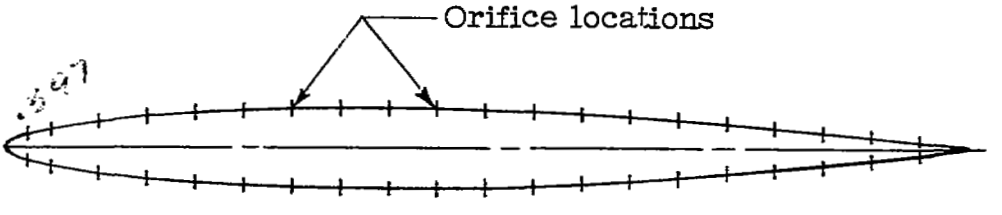

NACA 0009-44

Figure 2.- Airfoil profiles and orifice locations.

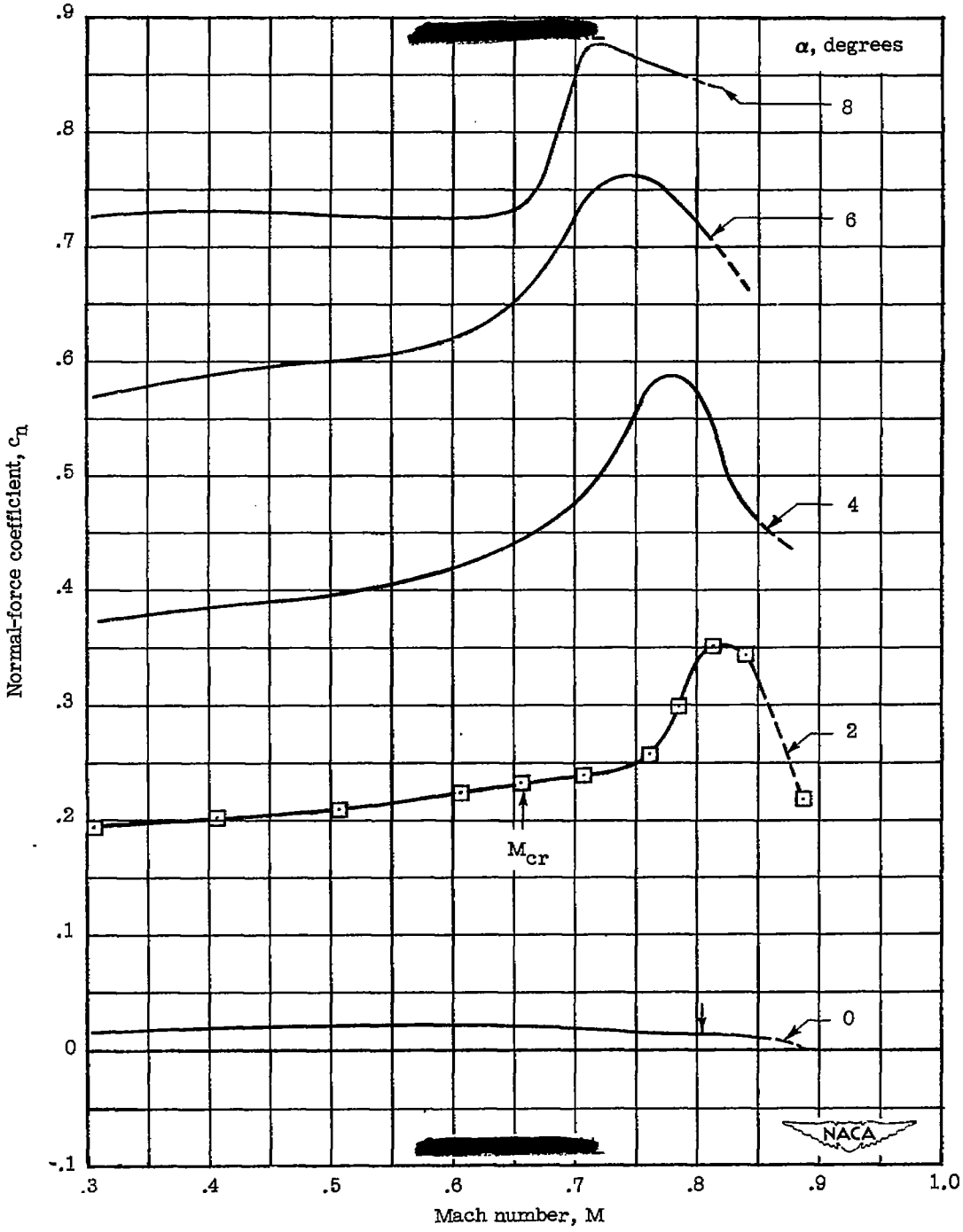

(a) NACA 0009-64.

Figure 3.- Effect of compressibility on normal-force characteristics of NACA 0009-64, 0009-54, and 0009-44 airfoils.

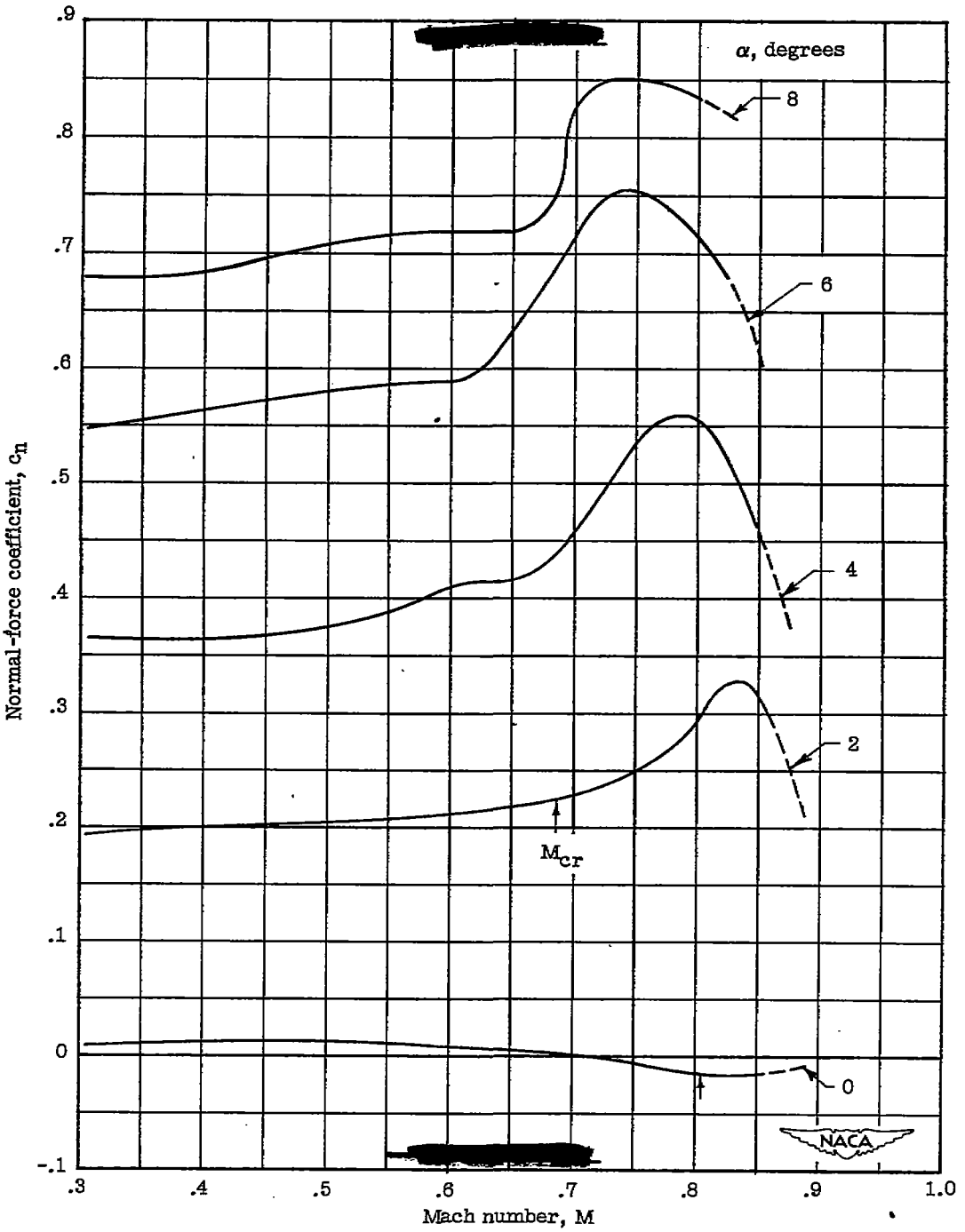

(b) NACA 0009-54.

Figure 3.- Continued.

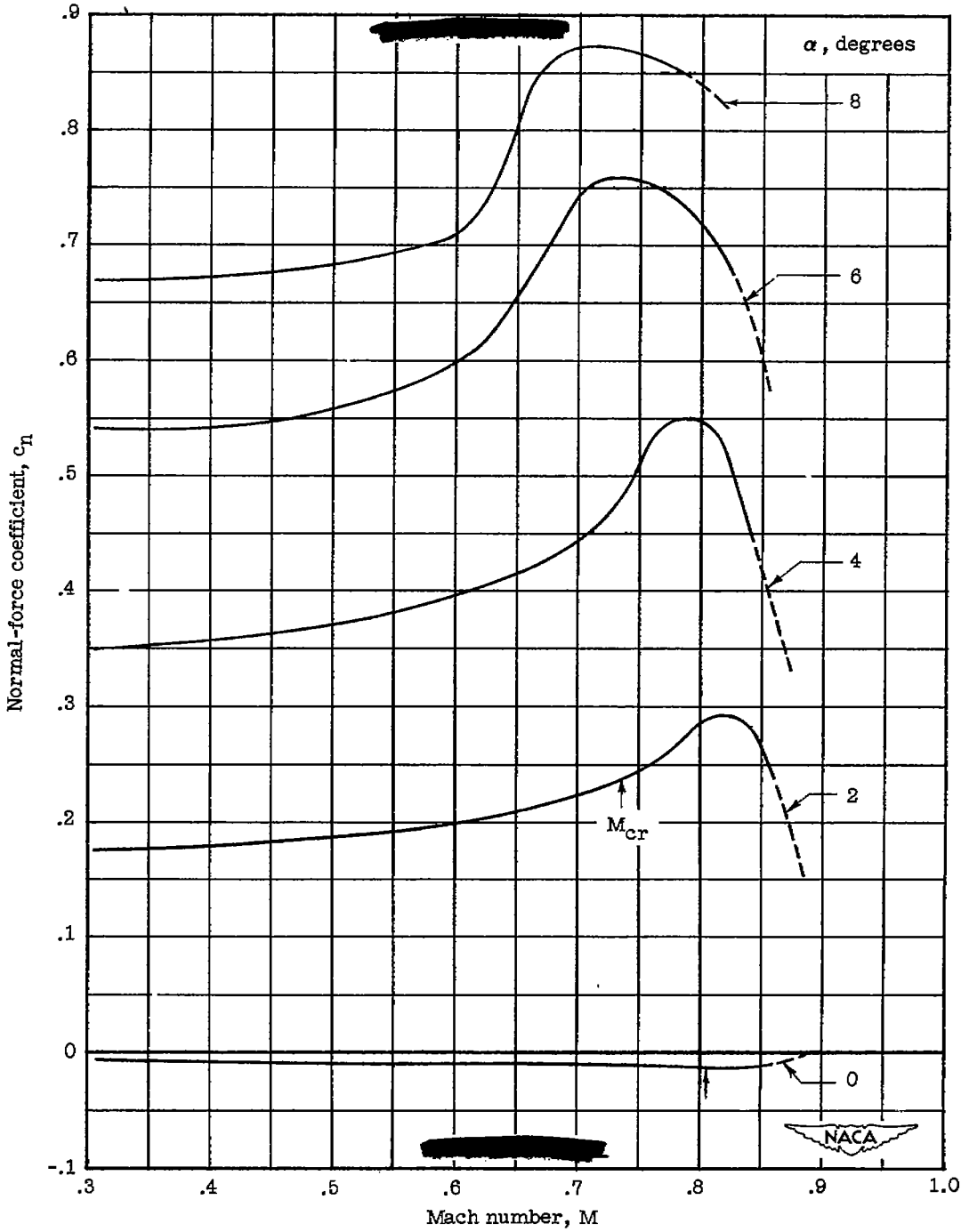

(c) NACA 0009-44.

Figure 3.- Concluded.

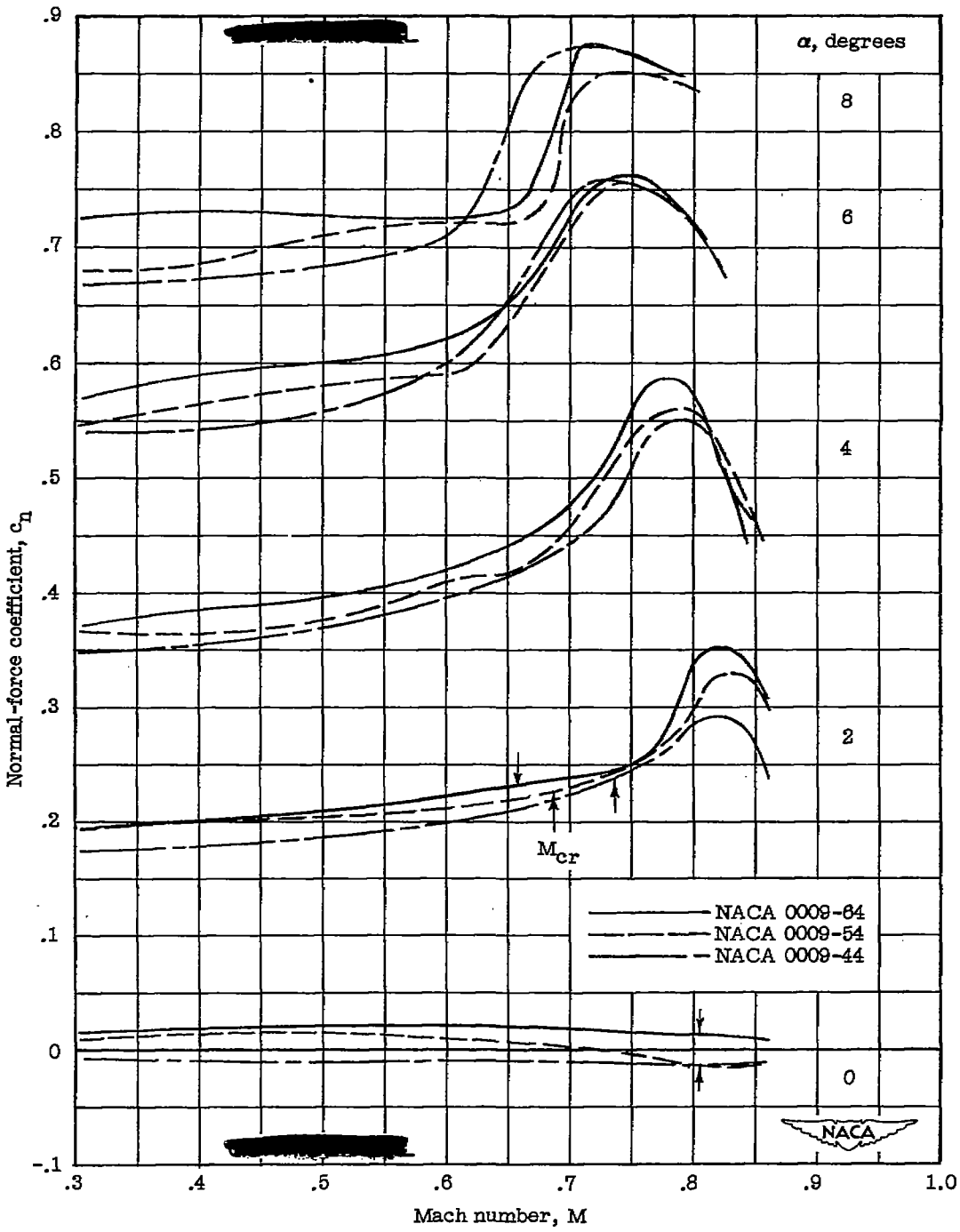

Figure 4.- Comparison of normal-force characteristics of NACA 0009-64, 0009-54, and 0009-44 airfoils.

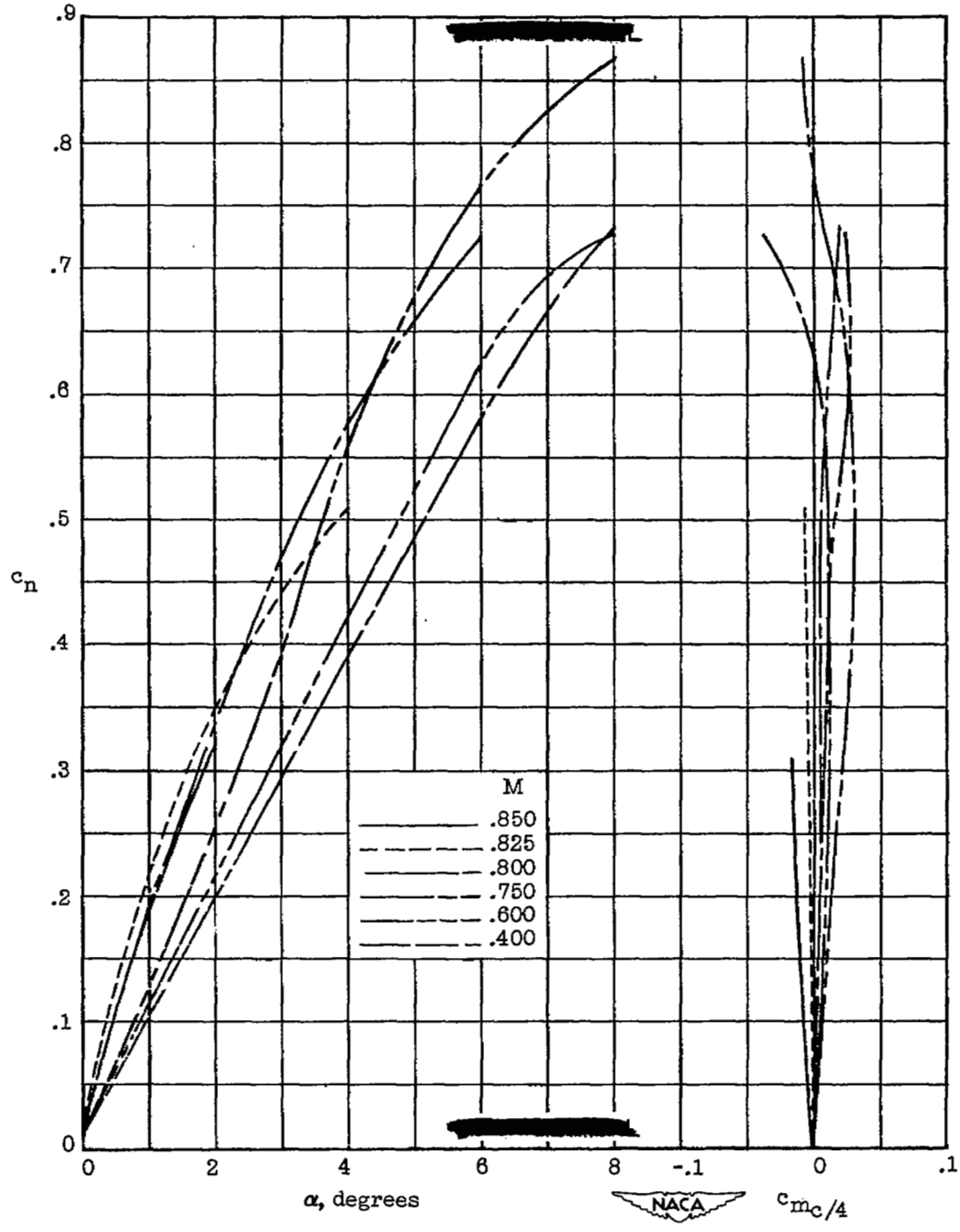

(a) NACA 0009-64.

Figure 5.- Normal-force and moment characteristics at constant Mach numbers for NACA 0009-64, 0009-54, and 0009-44 airfoils.

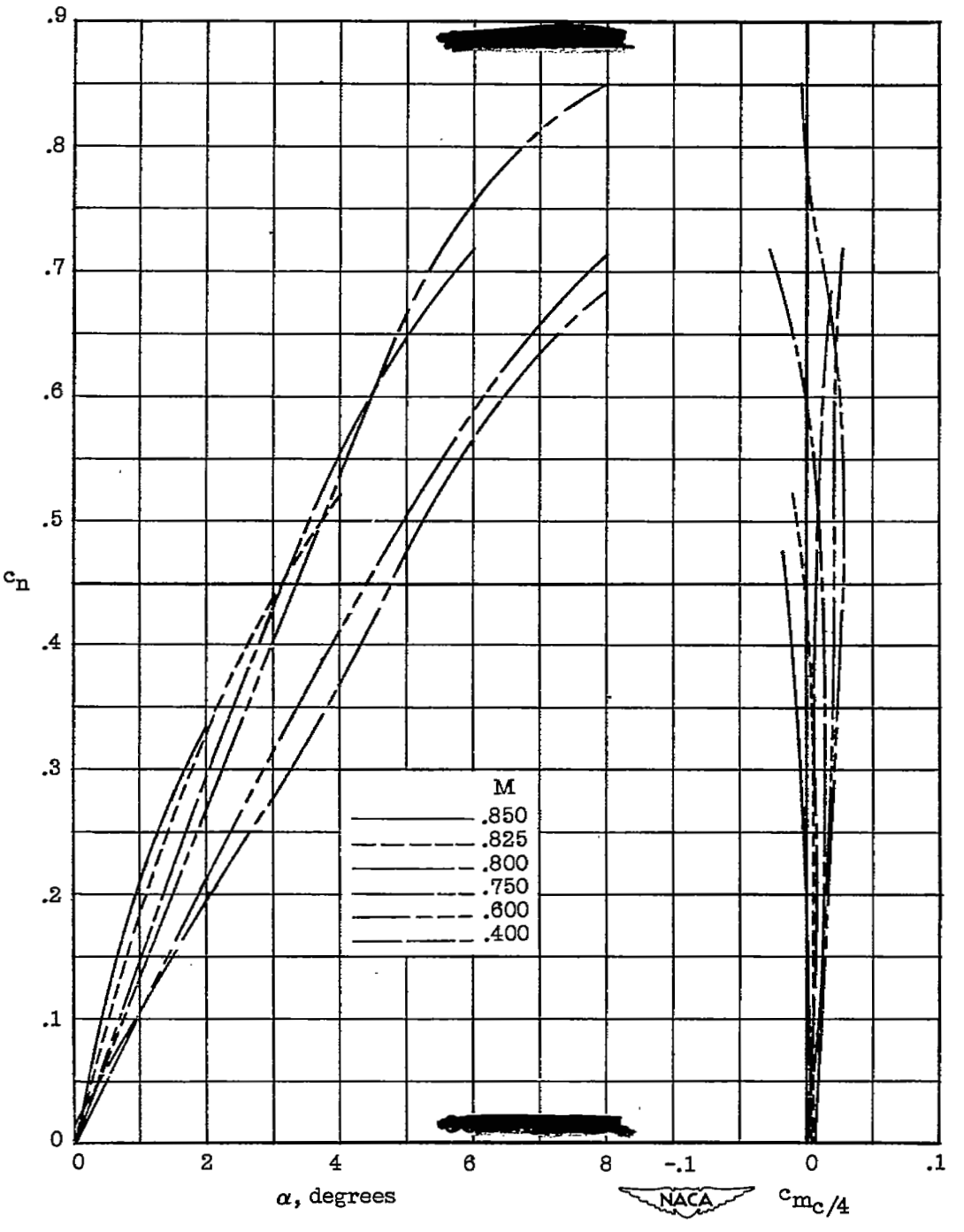

(b) NACA 0009-54.

Figure 5.- Continued.

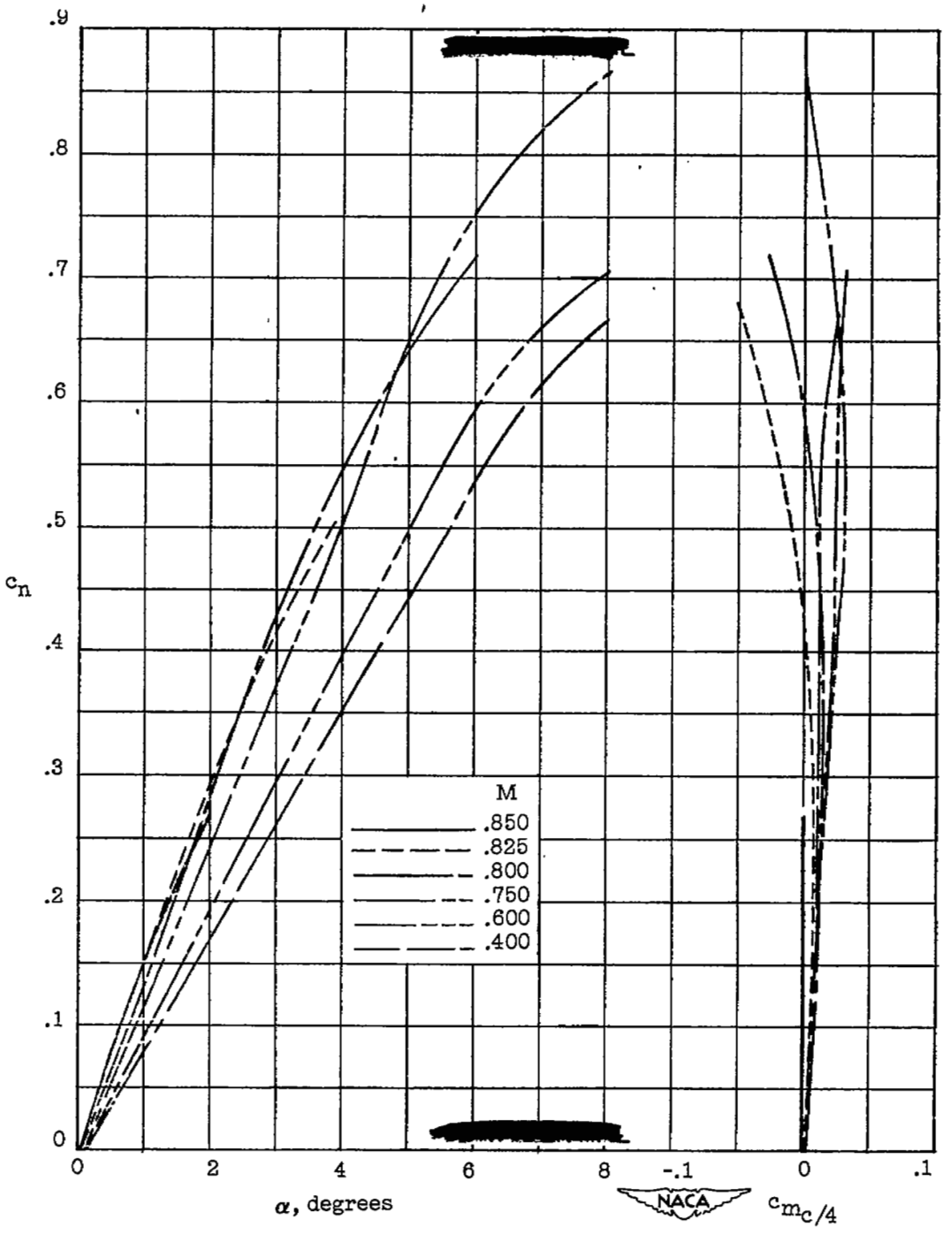

(c) NACA 0009-44.

Figure 5.- Concluded.

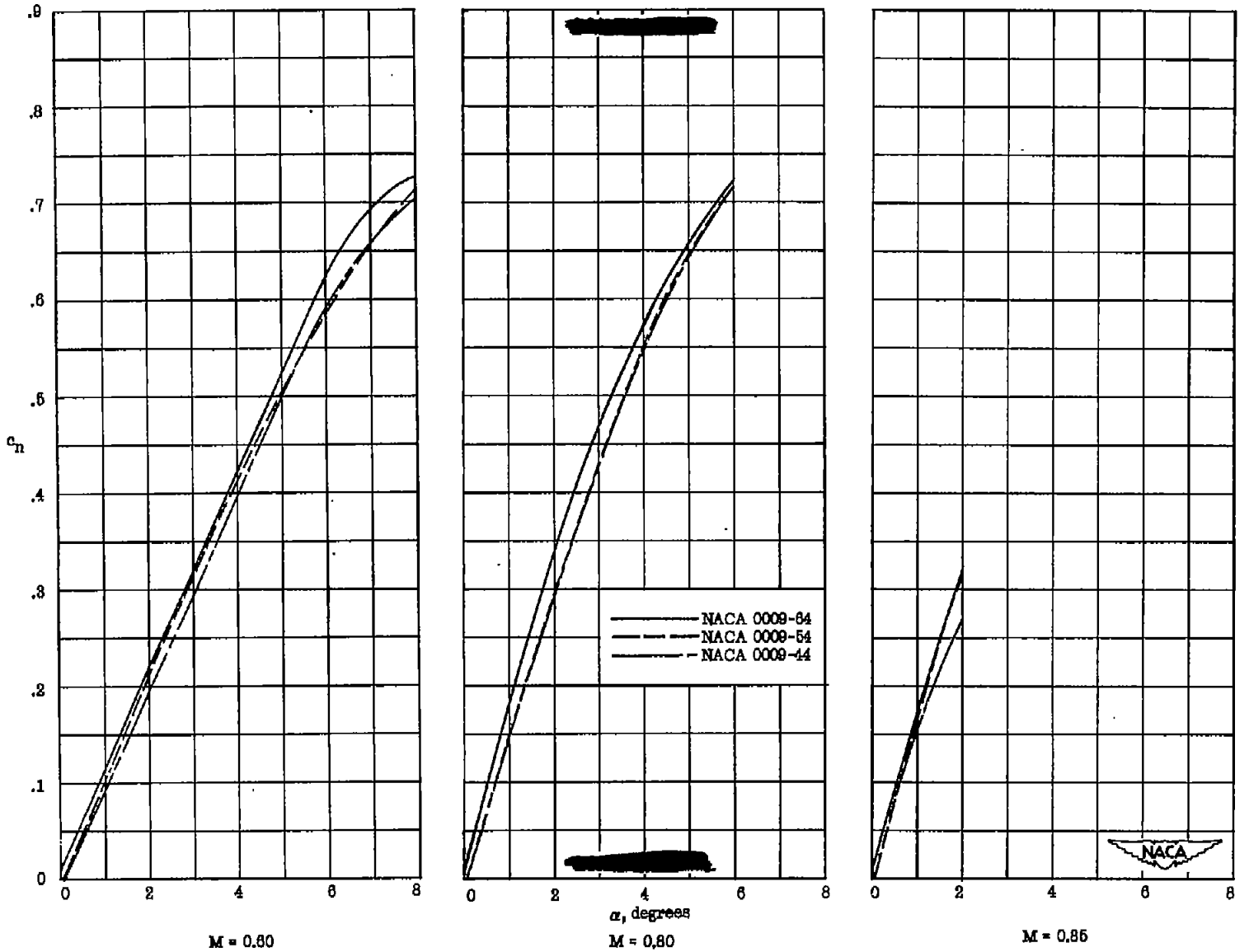

Figure 6.– Comparison of normal-force curves for the NACA 0009-64, 0009-54, and 0009-44 airfoils.

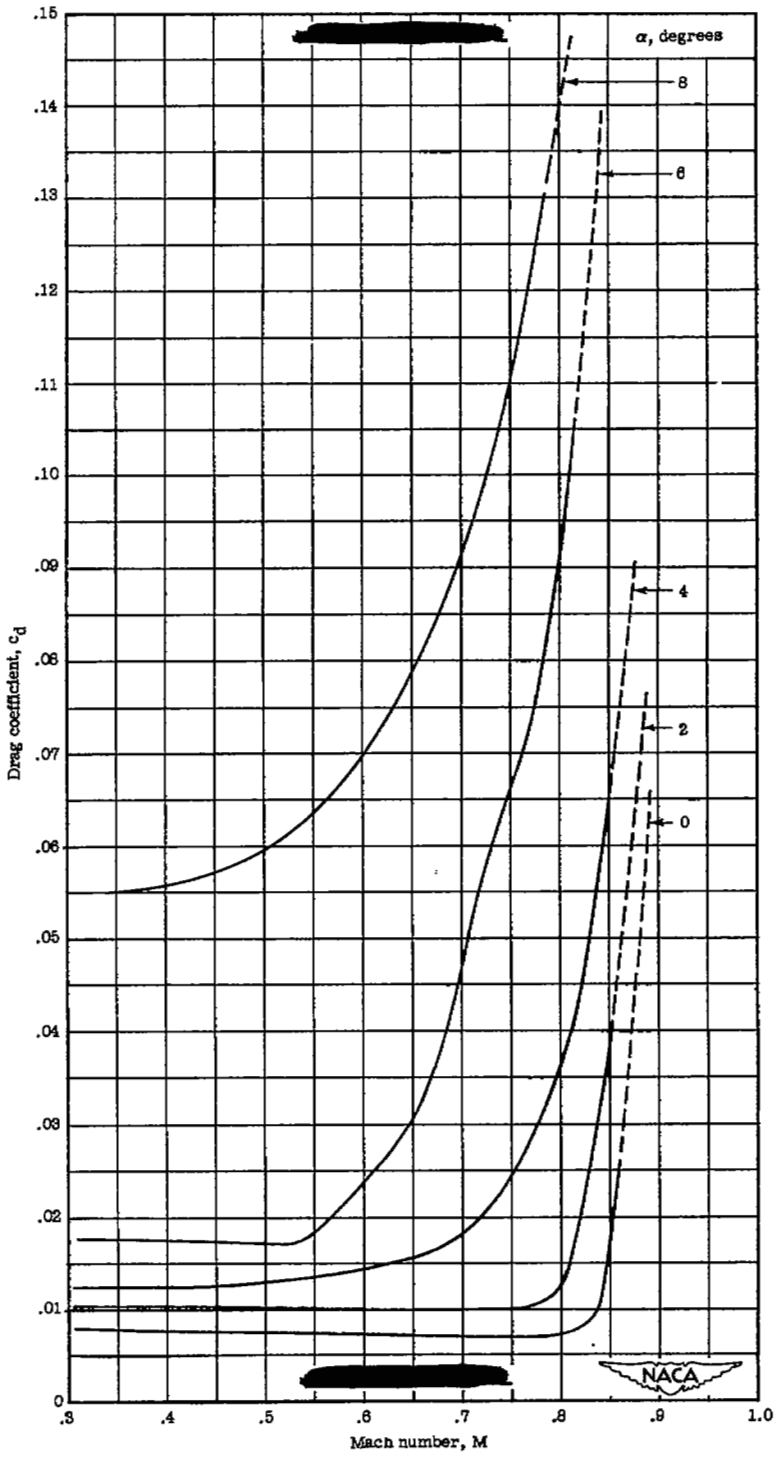

(a) NACA 0009-64.

Figure 7.- Effect of compressibility on drag characteristics of NACA 0009-64, 0009-54, and 0009-44 airfoils.

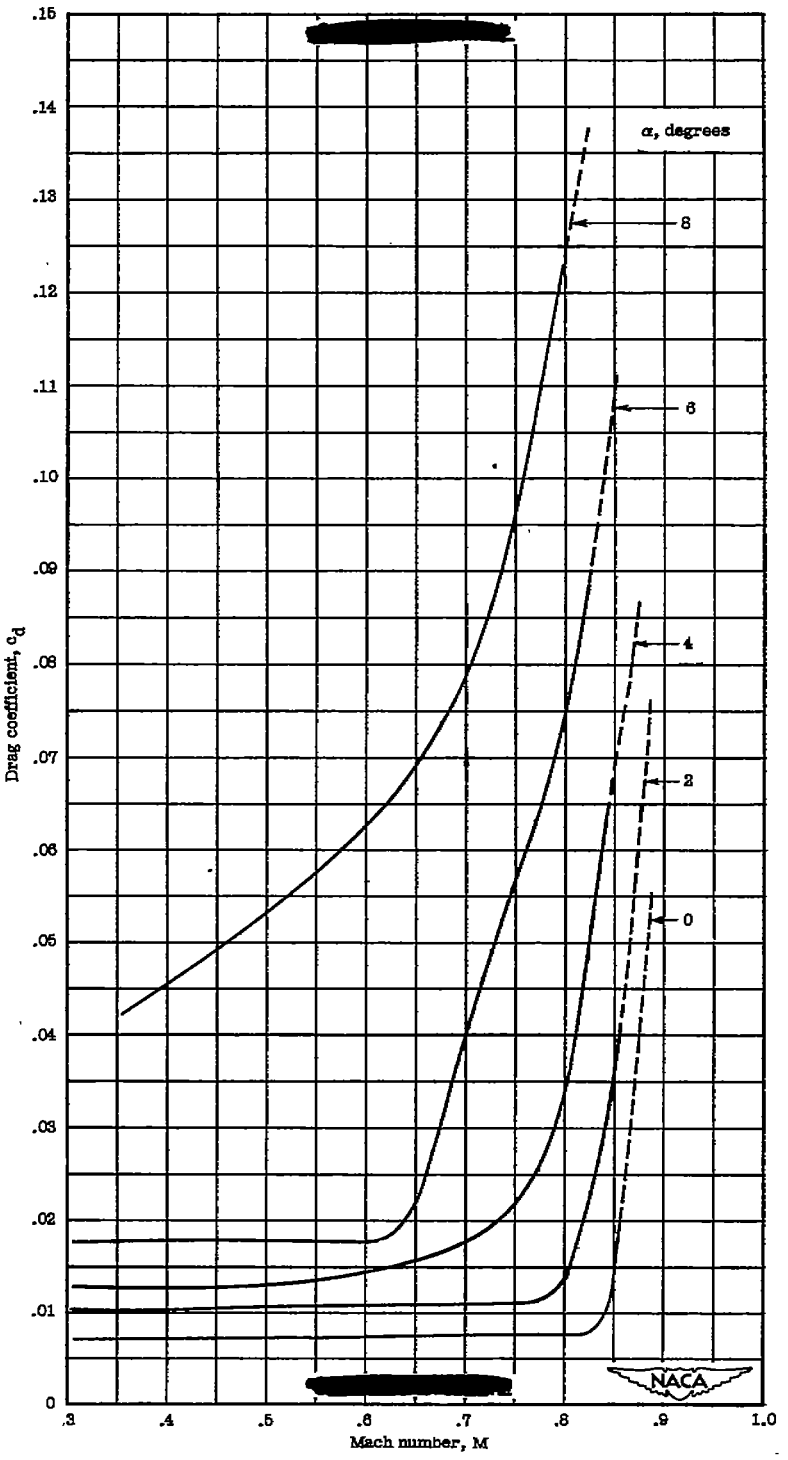

(b) NACA 0009-54.

Figure 7.- Continued.

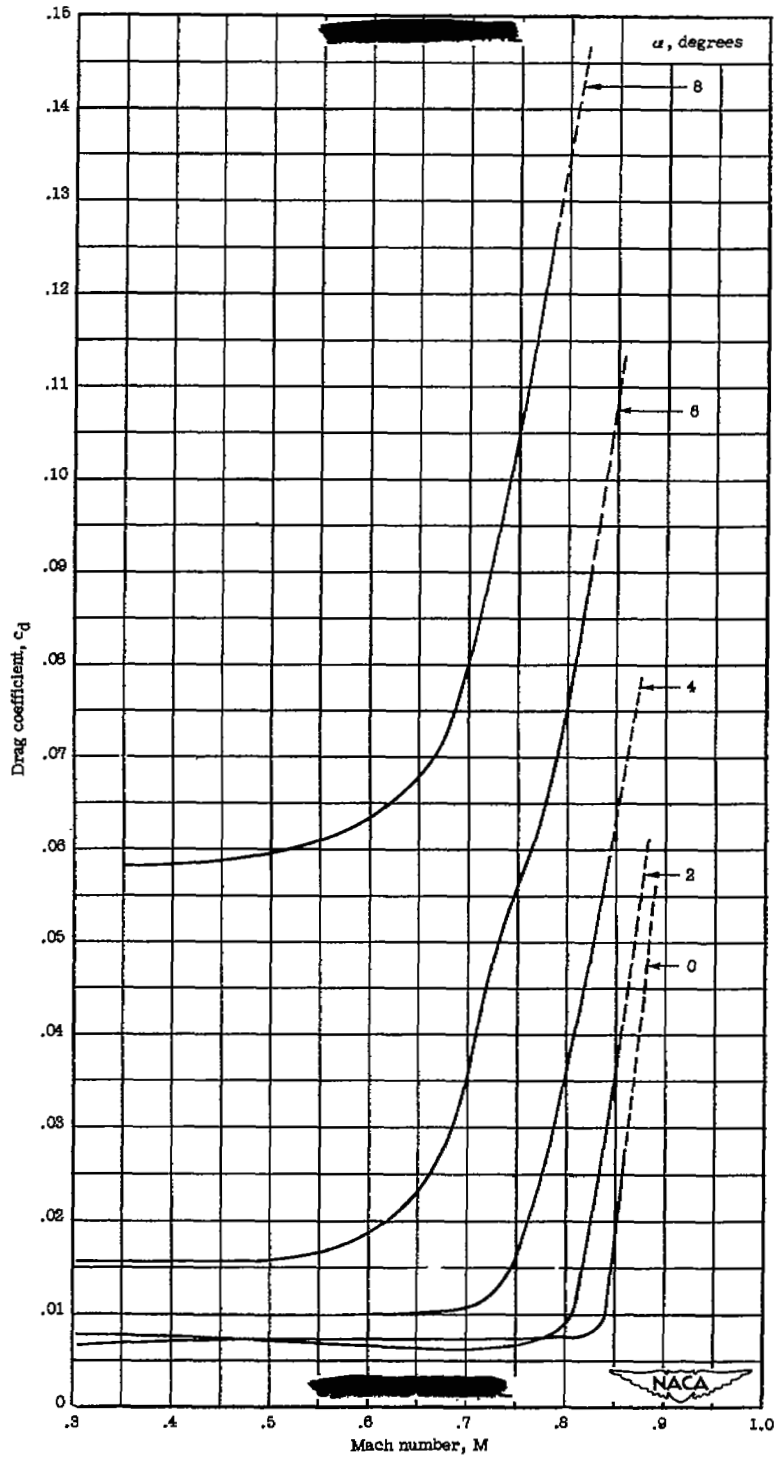

(c) NACA 0009-44.

Figure 7.- Concluded.

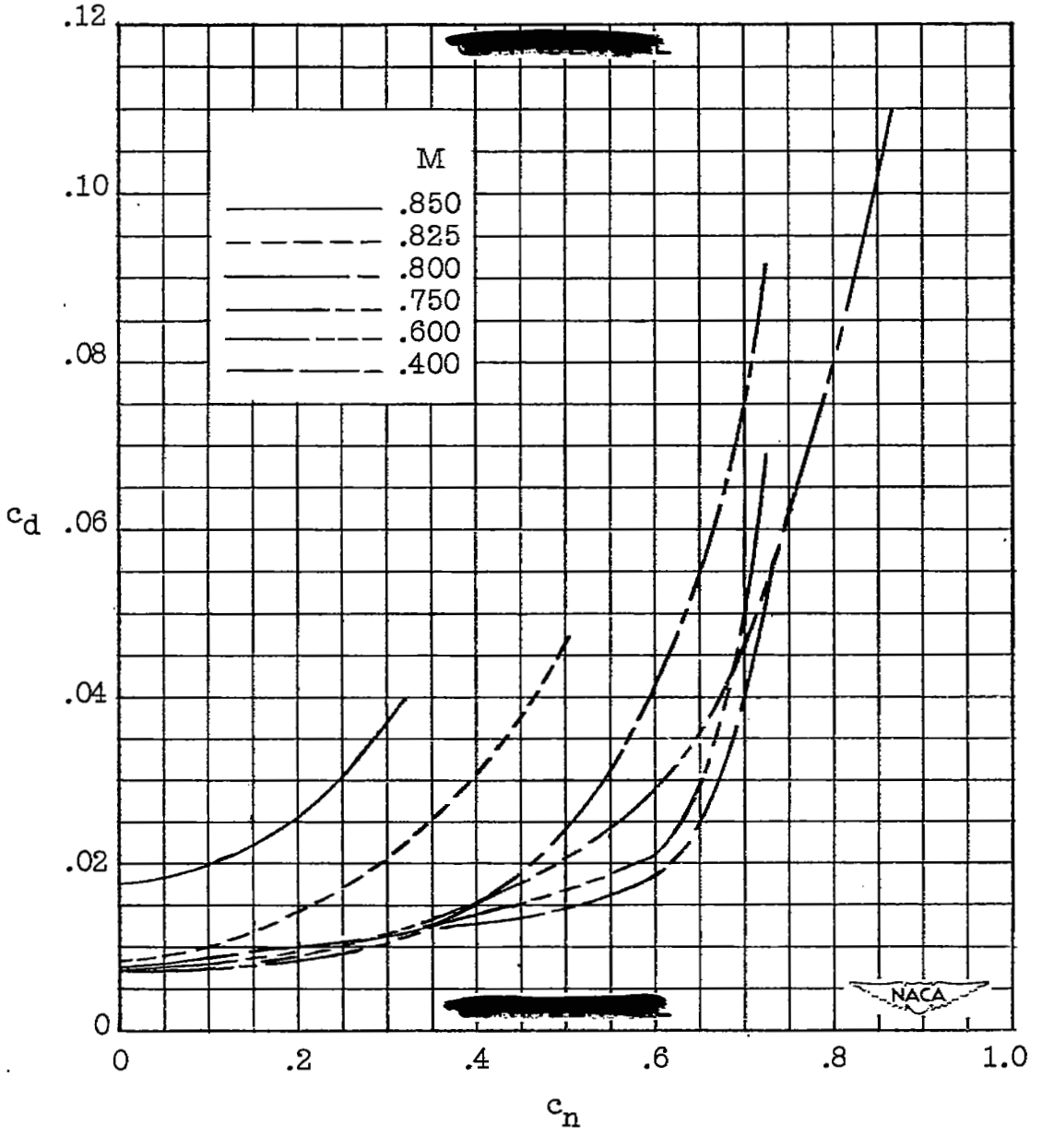

(a) NACA 0009-64.

Figure 8.- Polar diagrams at constant Mach numbers for NACA 0009-64, 0009-54, and 0009-44 airfoils.

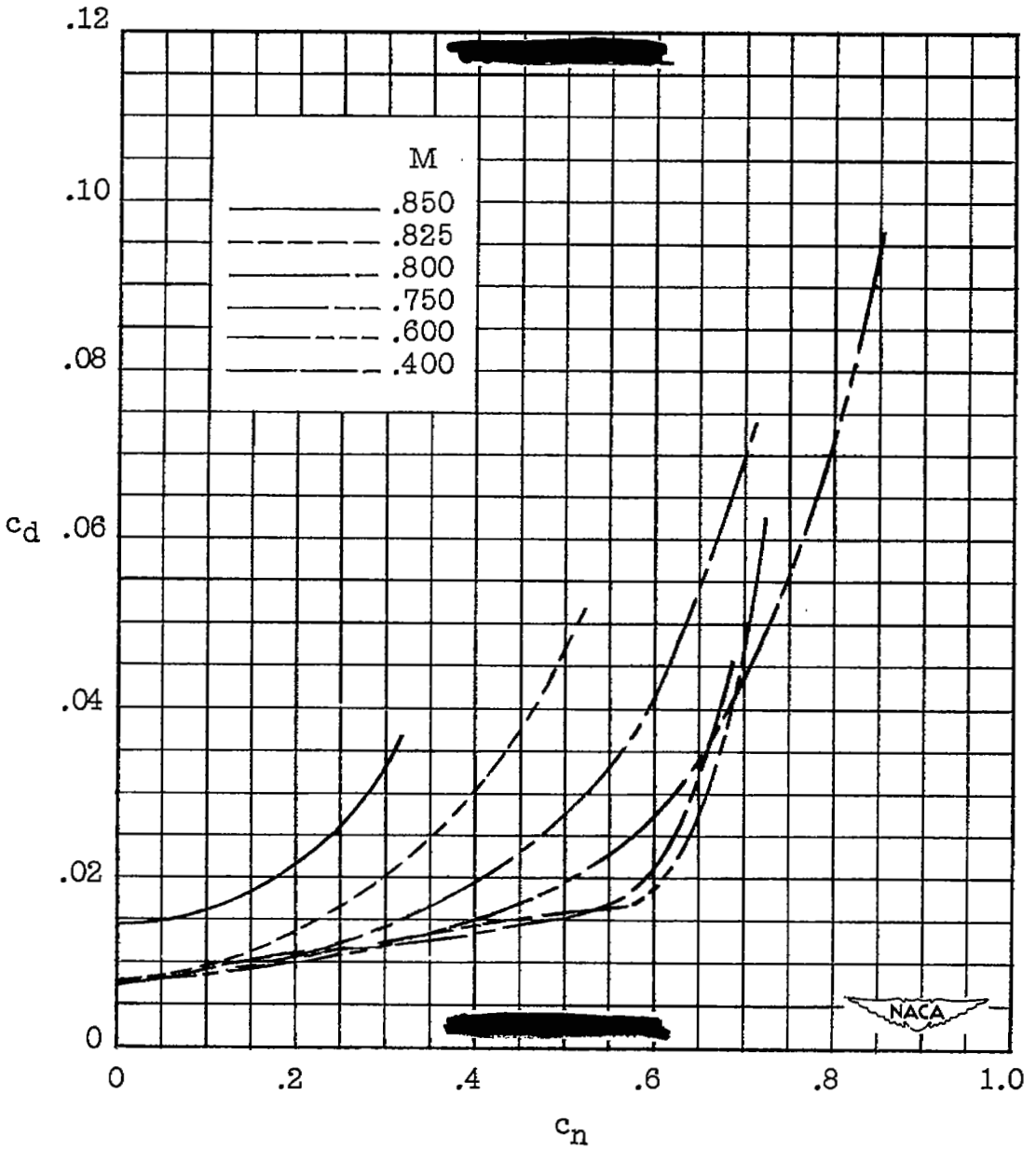

(b) NACA 0009-54.

Figure 8.- Continued.

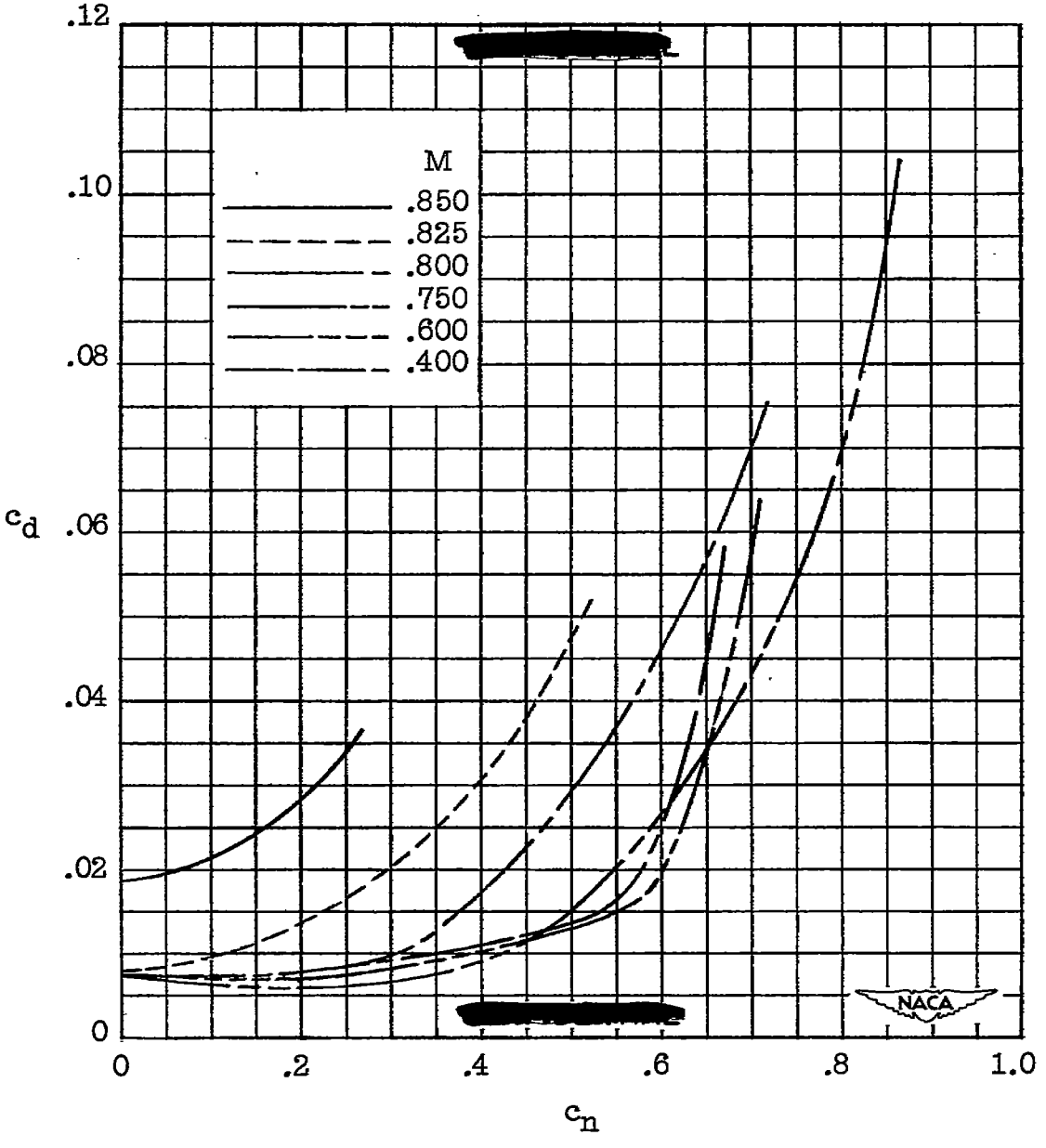

(c) NACA 0009-44.

Figure 8.- Concluded.

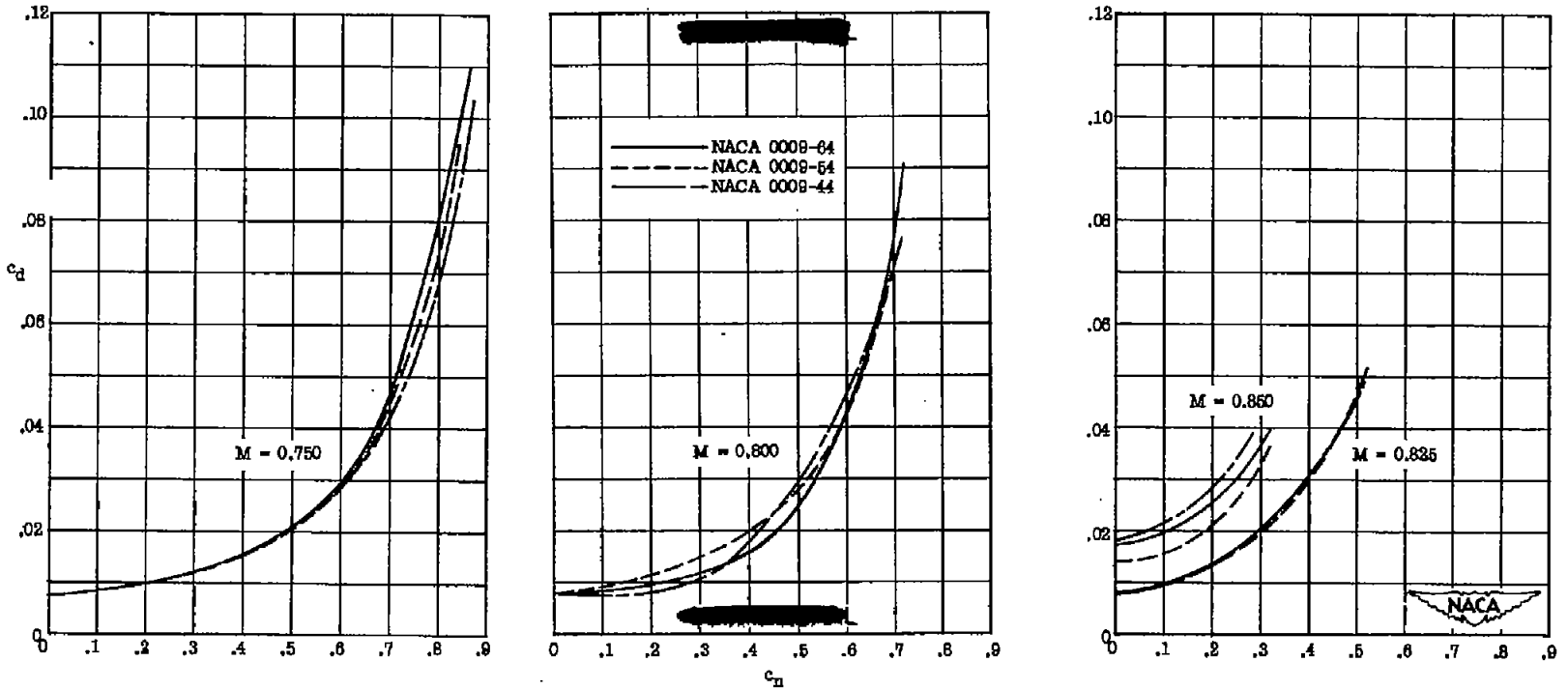

Figure 9.- Comparison of drag polars for the NACA 0009-64, 0009-54, and 0009-44 airfoils.

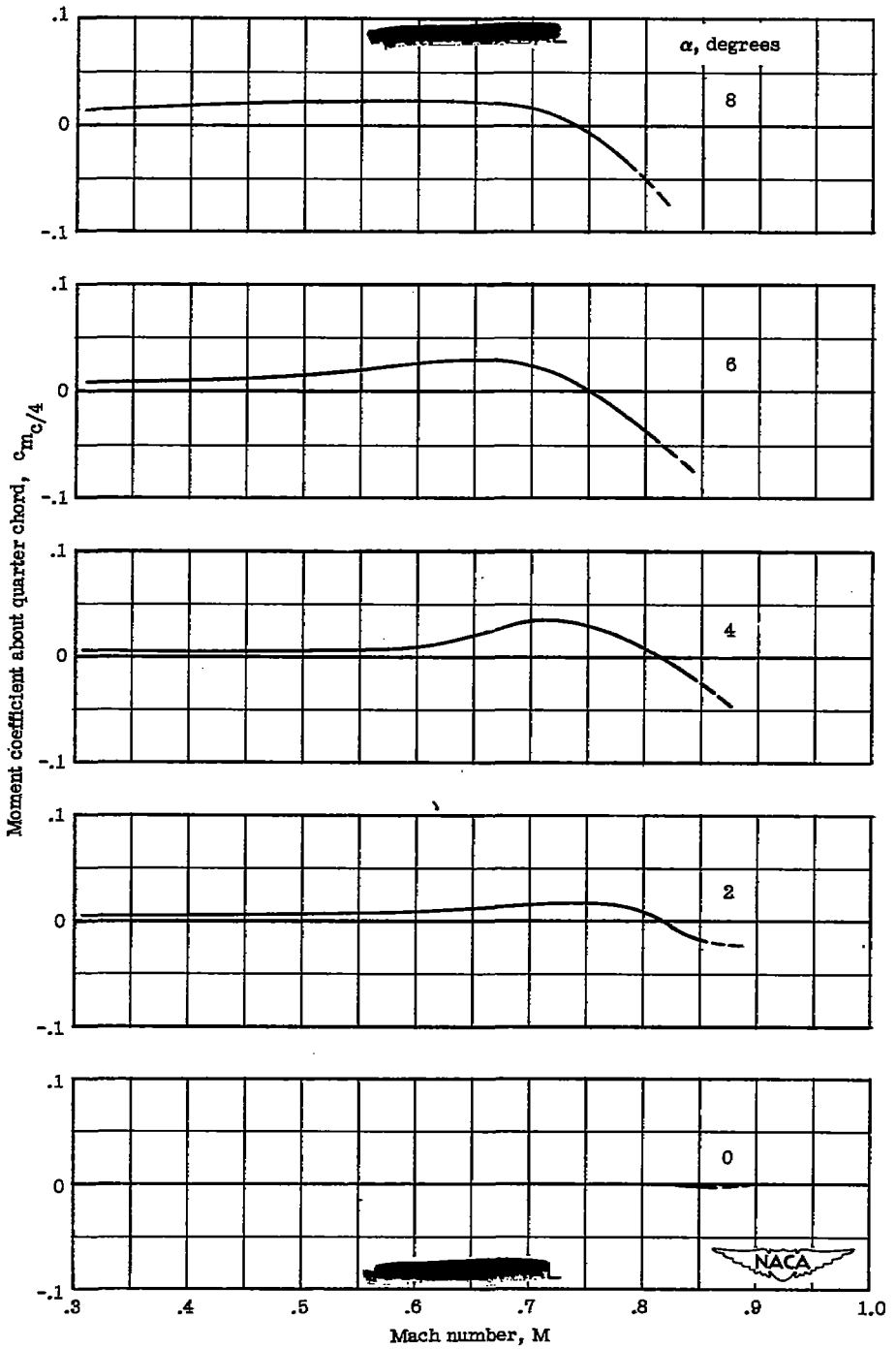

(a) NACA 0009-64.

Figure 10.- Effect of compressibility on quarter-chord moment characteristics of NACA 0009-64, 0009-54, and 0009-44 airfoils.

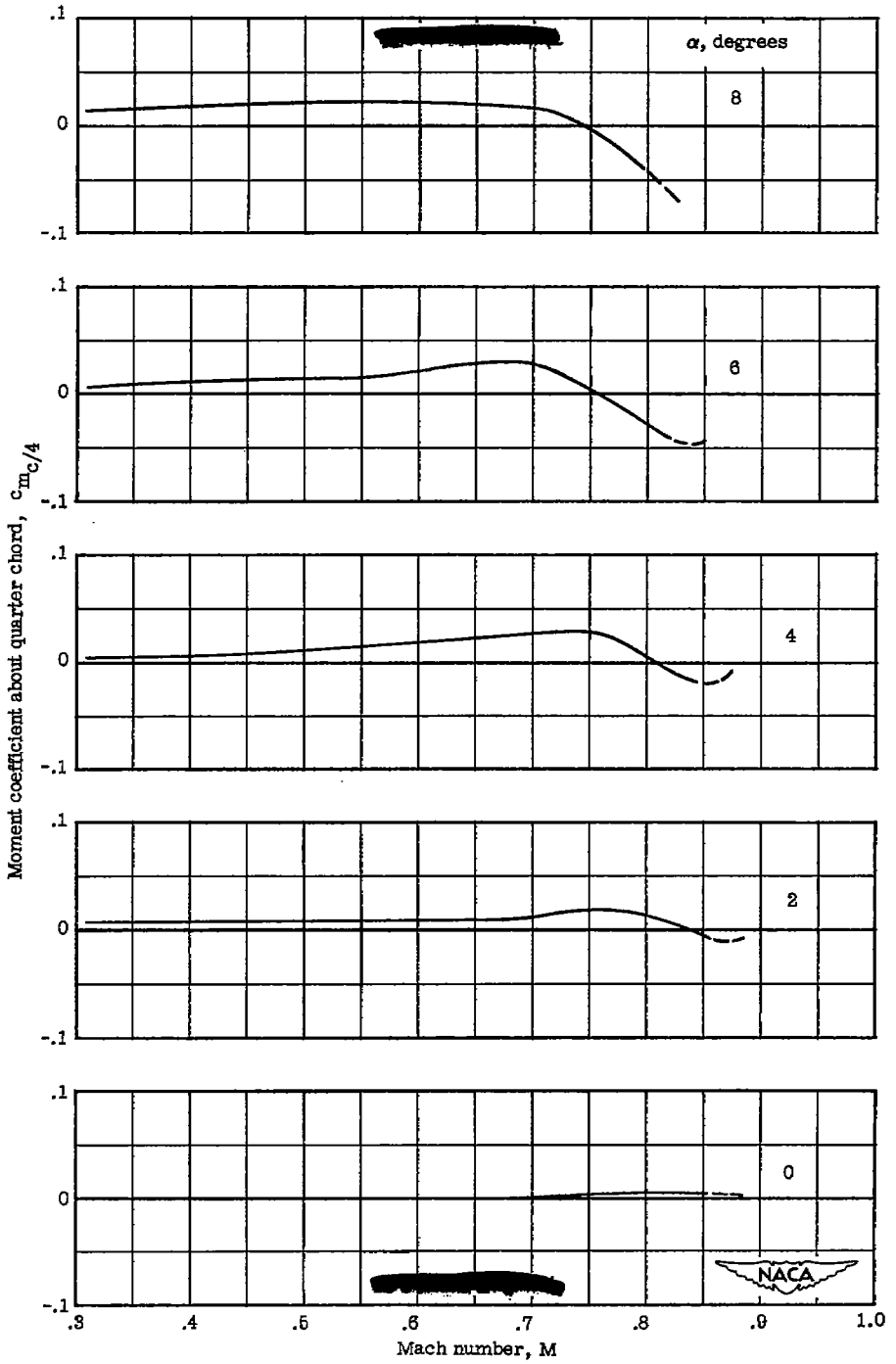

(b) NACA 0009-54.

Figure 10.- Continued.

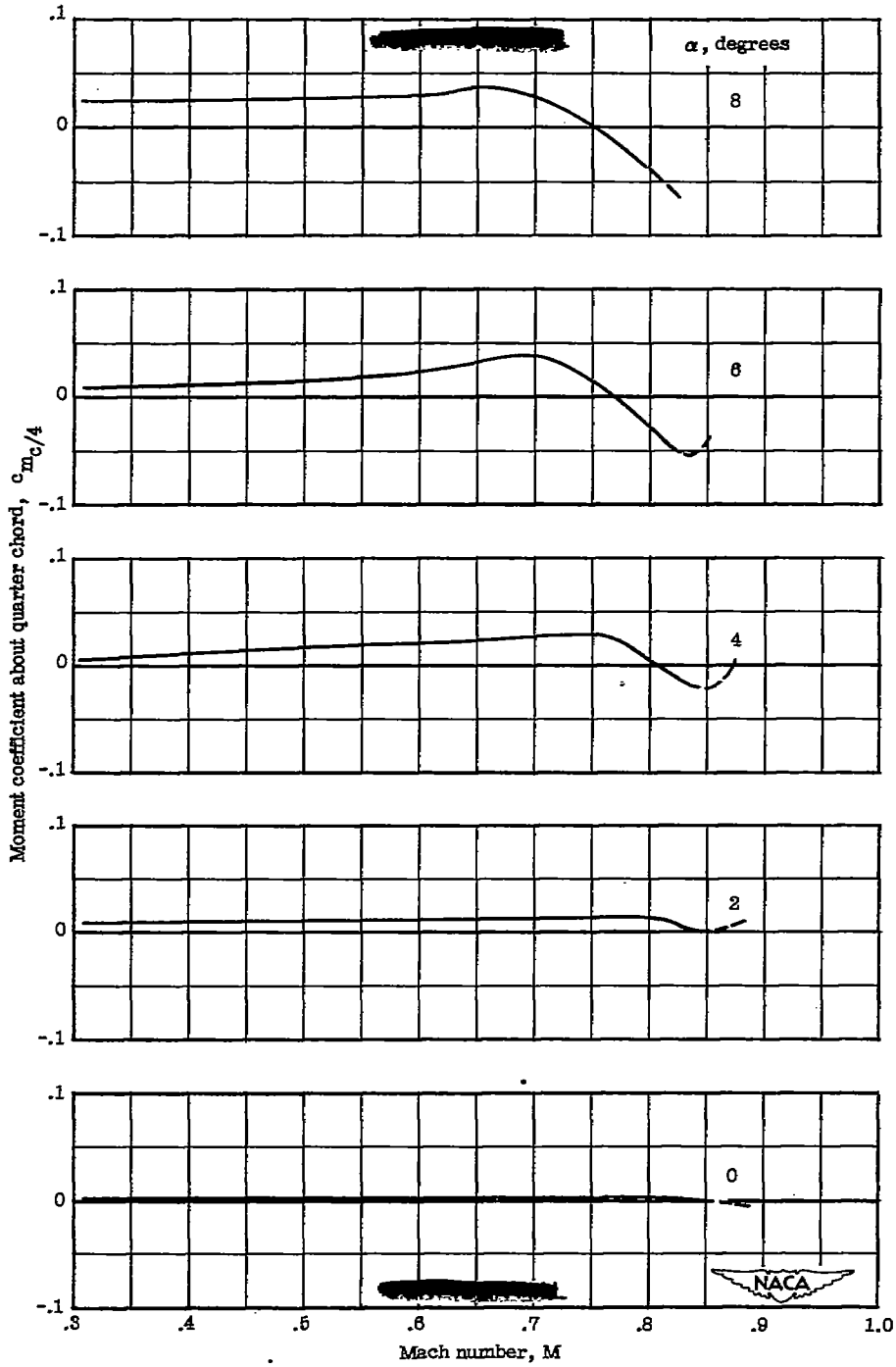

(c) NACA 0009-44.

Figure 10.- Concluded.

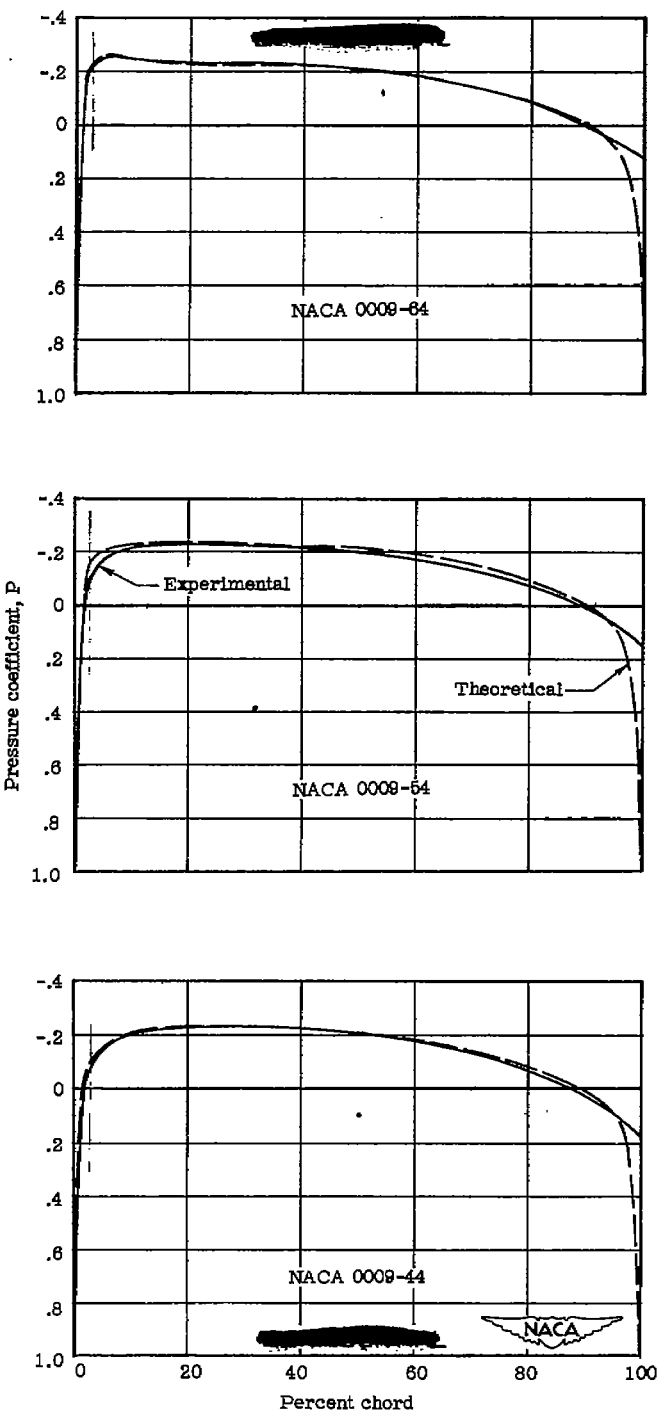

Figure 11.- Comparison of theoretical and experimental pressure-distribution diagrams of NACA 0009-64, 0009-54, and 0009-44 airfoils. $\alpha = 0^{\circ}$; M = 0.00.

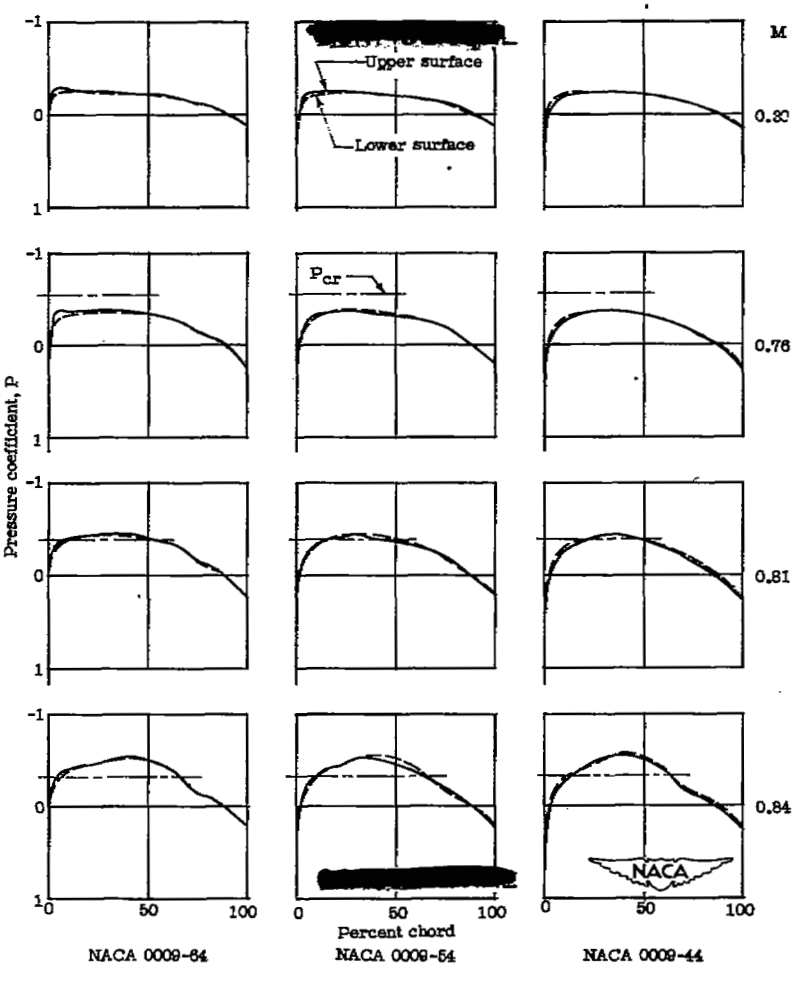

(a) $\alpha = 0^{\circ}$.

Figure 12.- Pressure distributions for NACA 0009-64, 0009-54, and 0009-44 airfoils.

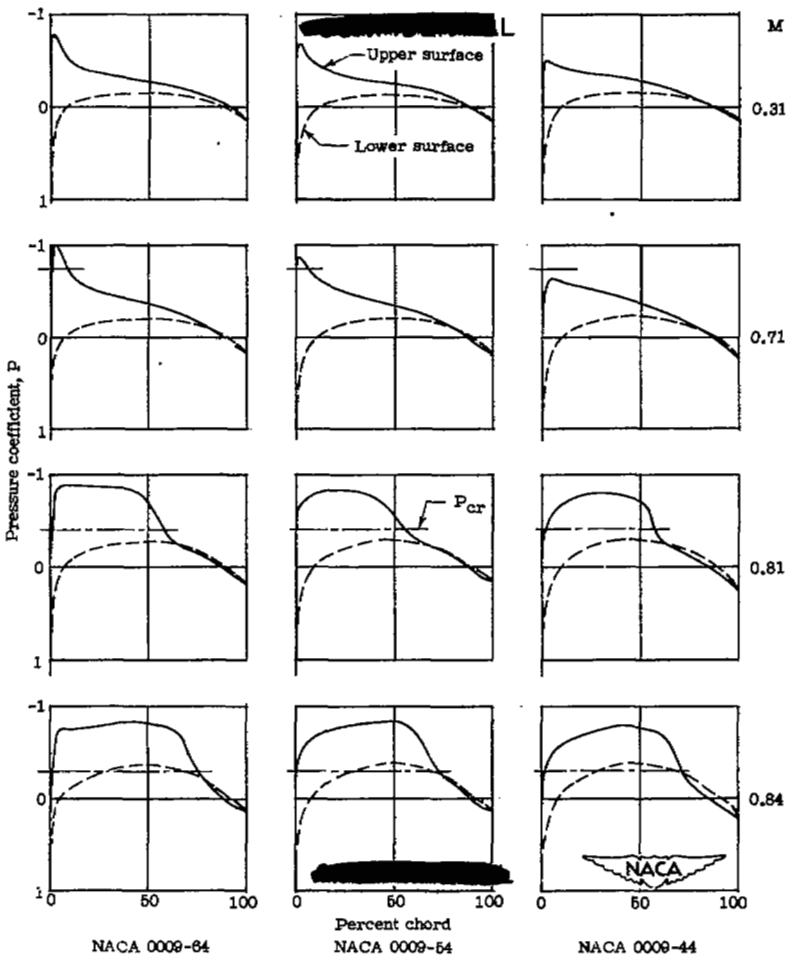

(b) $\alpha = 2^{\circ}$.

Figure 12.- Continued.

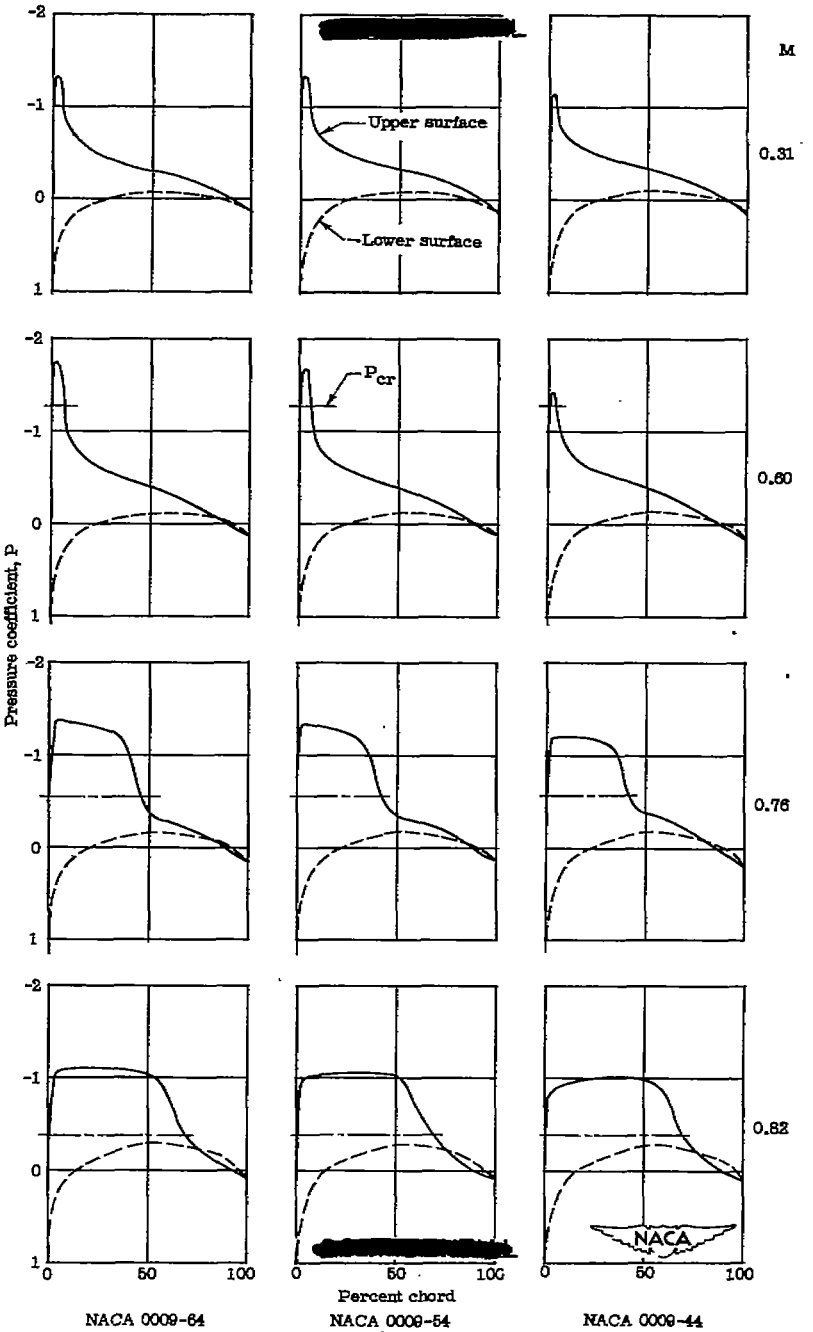

(c) $\alpha = 4^\circ$.

Figure 12.- Continued.

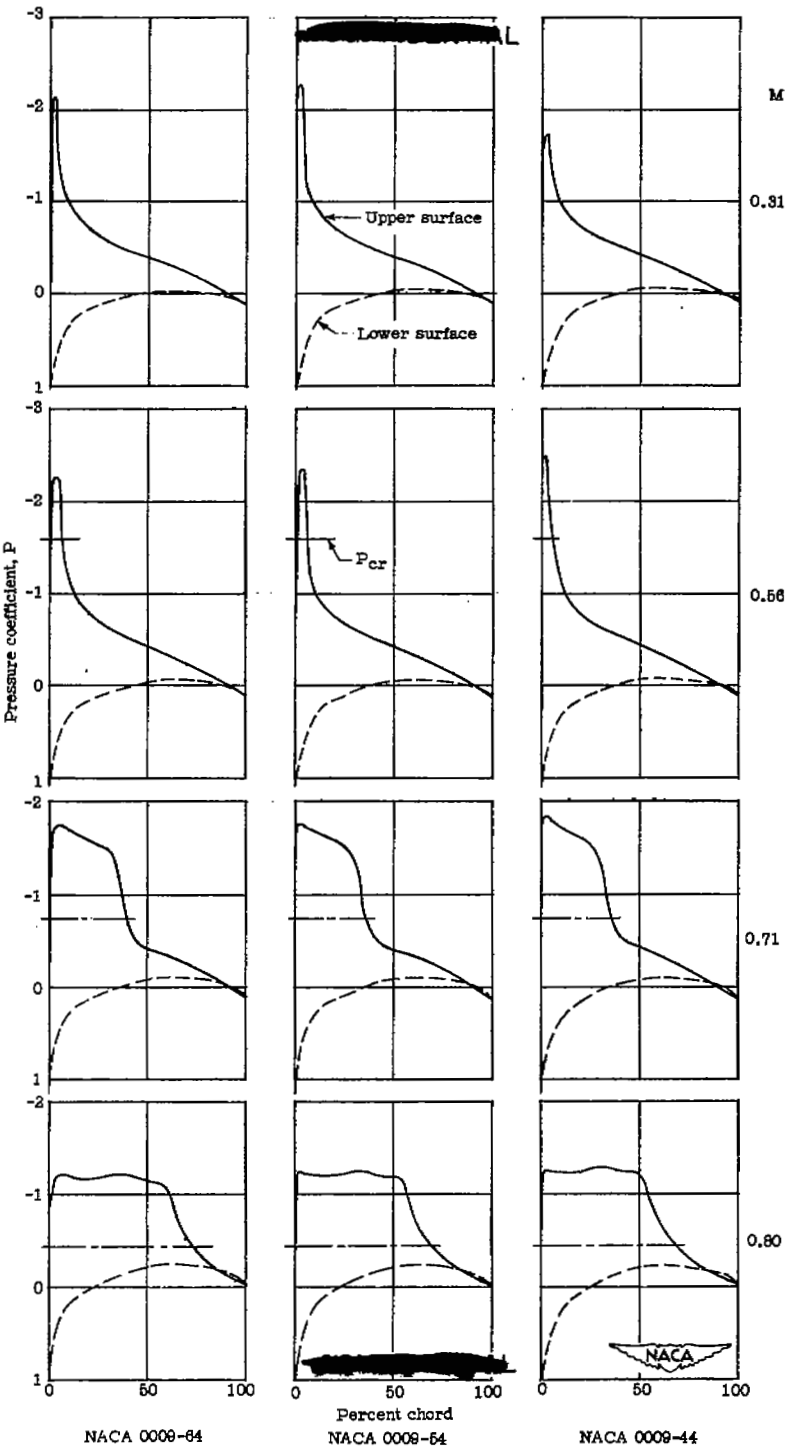

(d) $\alpha = 6^{\circ}$.

Figure 12.– Continued.

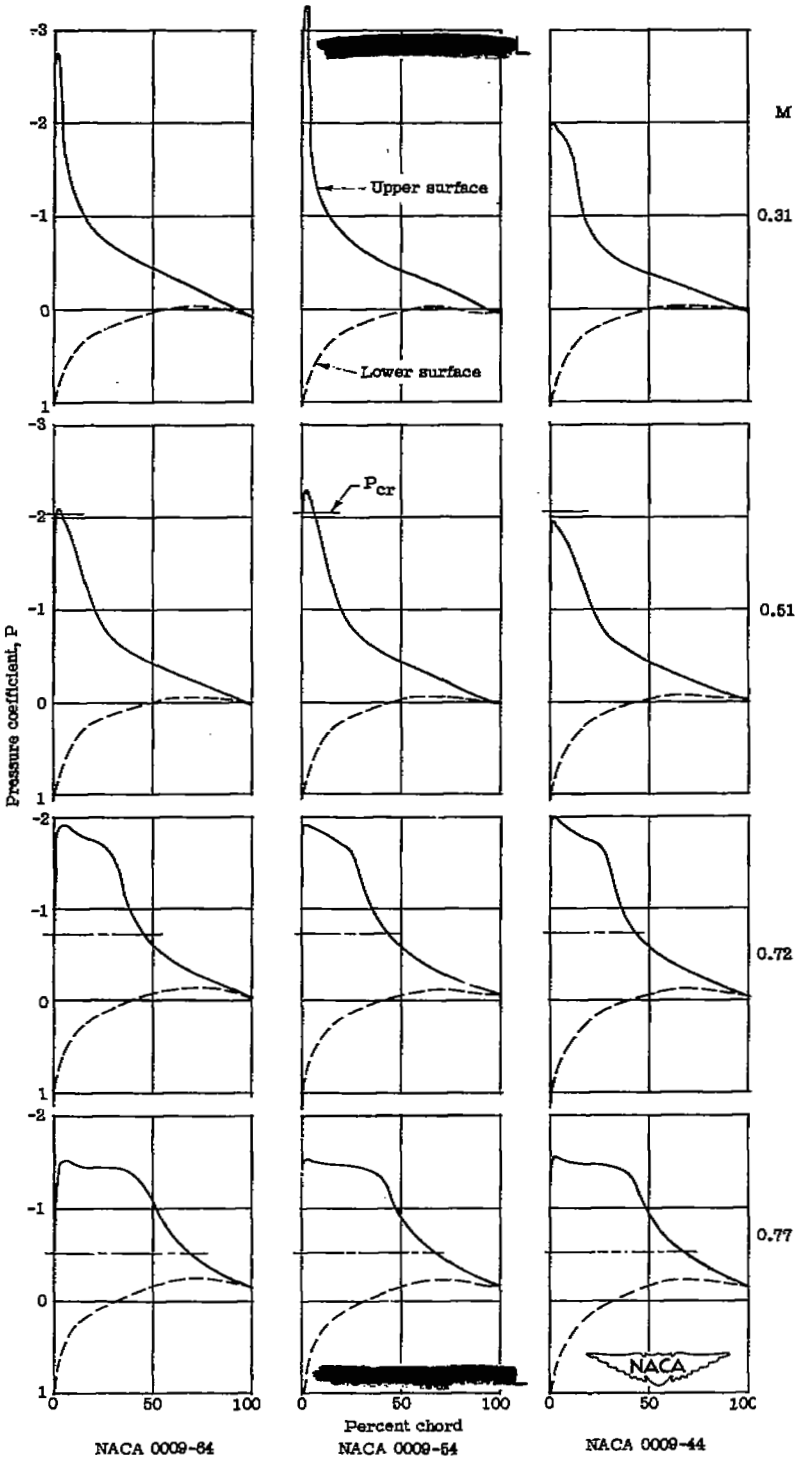

(e) $\alpha = 8^{\circ}$.

Figure 12.– Concluded.

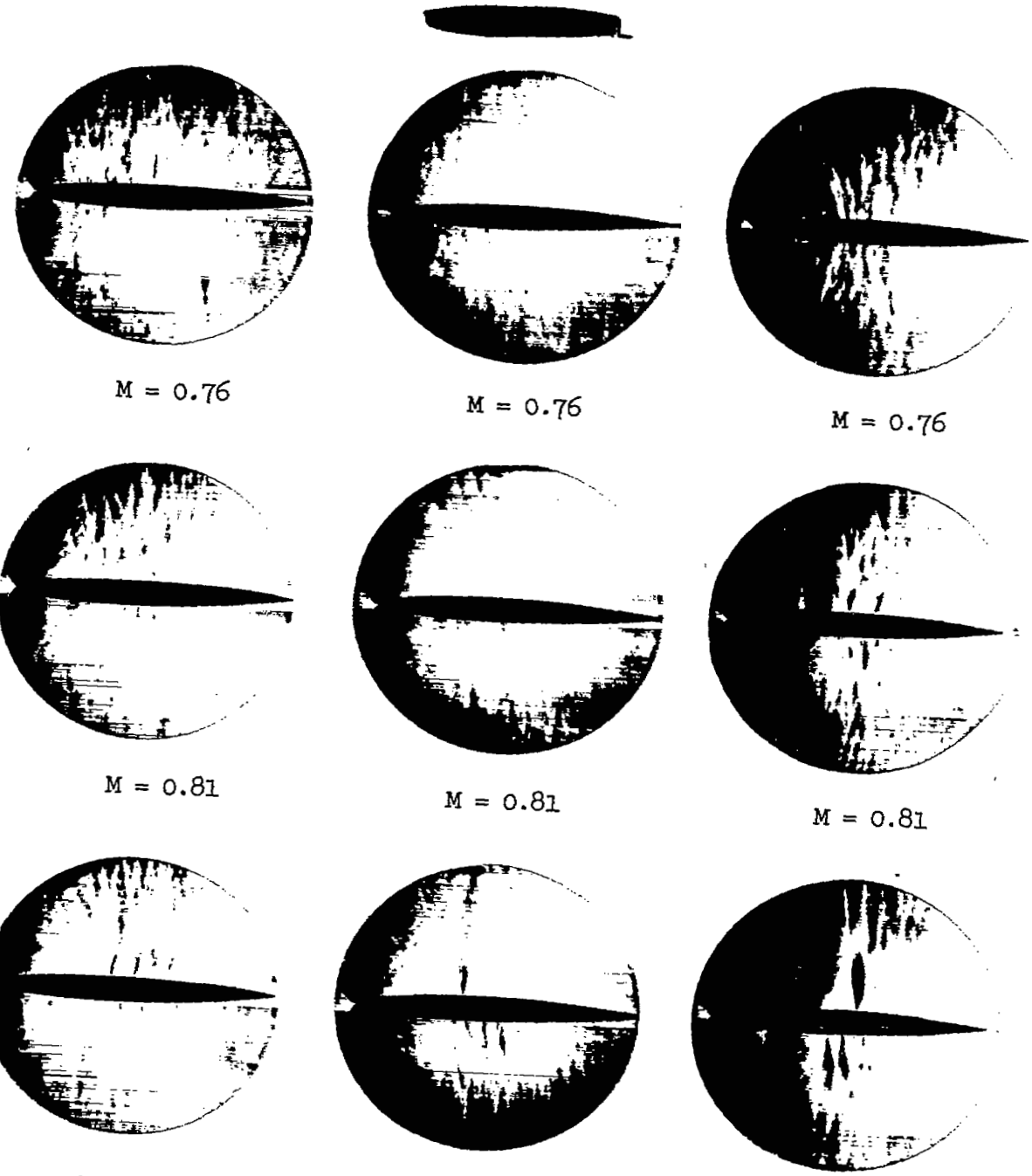

(a) $\alpha = 0°$.

Figure 13.- Schlieren photographs of NACA 0009-64, 0009-54, and 0009-44 airfoils.

NACA L-63558

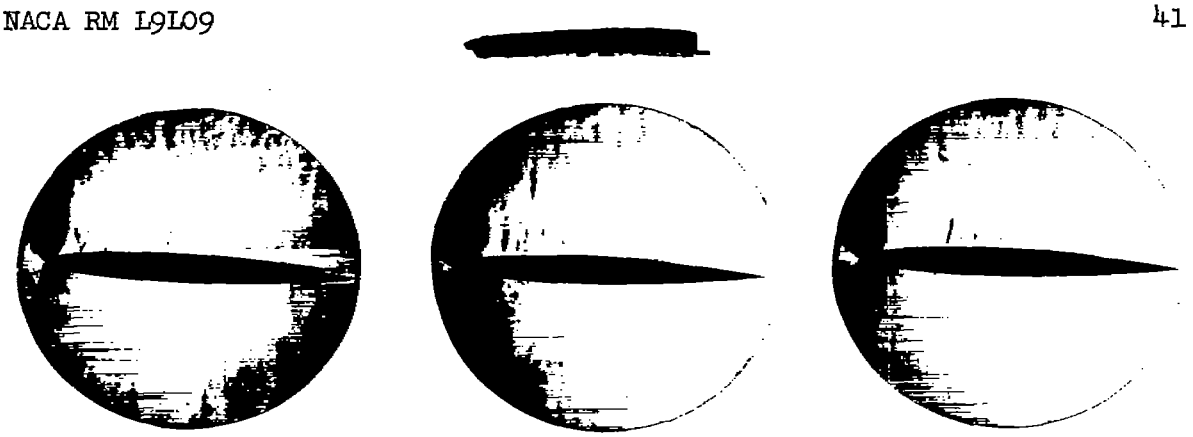

M = 0.76 M = 0.76 M = 0.76

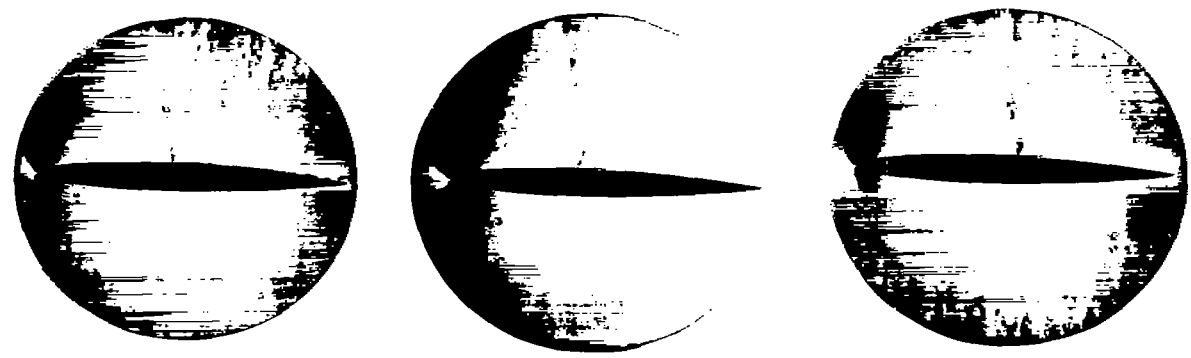

M = 0.81 M = 0.81 M = 0.81

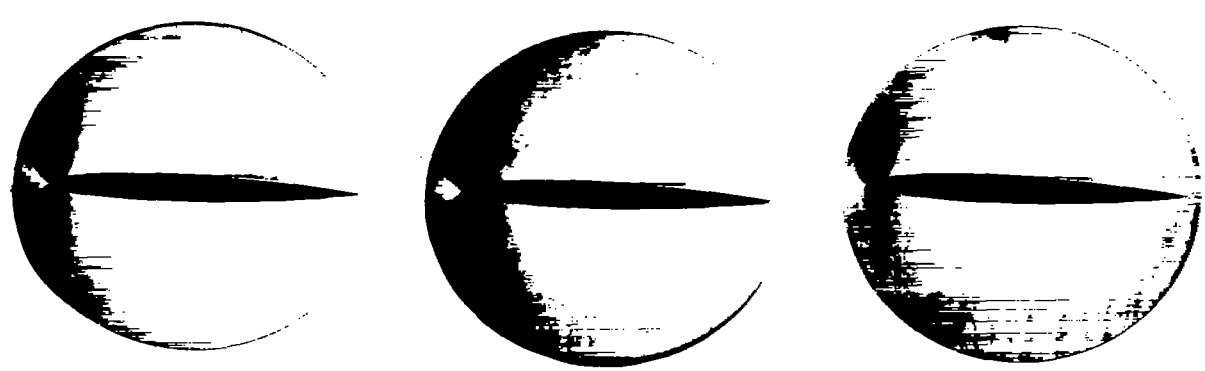

M = 0.84 M = 0.84 M = 0.84

NACA 0009-64 NACA 0009-54 NACA 0009-44

(b) $\alpha = 2^\circ$.

Figure 13.- Continued. L-63559

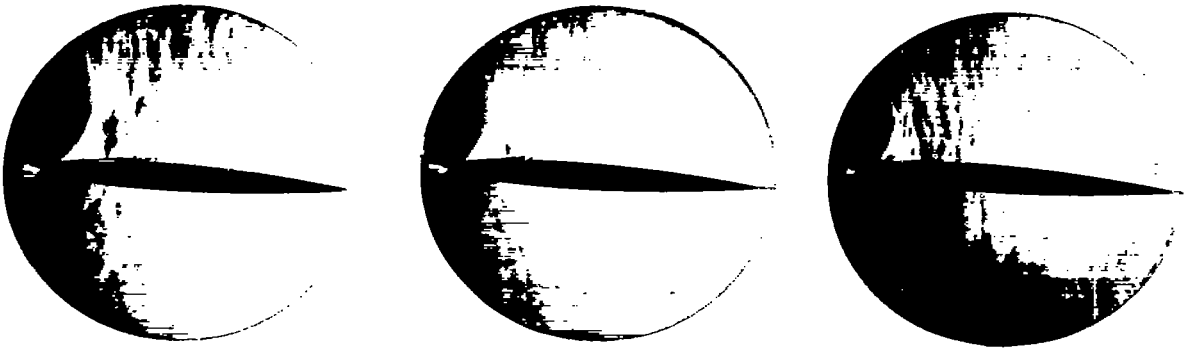

M = 0.70 M = 0.70 M = 0.70

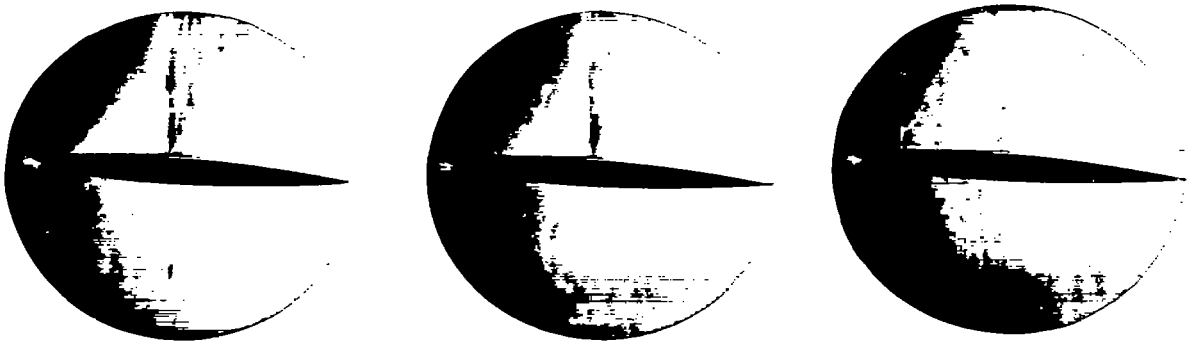

M = 0.76 M = 0.76 M = 0.76

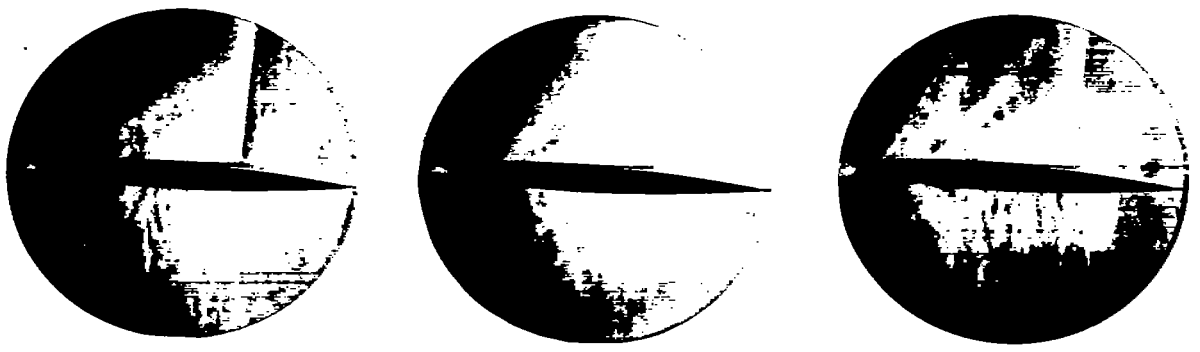

M = 0.81 M = 0.81 M = 0.81

NACA 0009-64 NACA 0009-54 NACA 0009-44

(c) $\alpha = 4^\circ$.

Figure 13.- Continued.

NACA L-63560

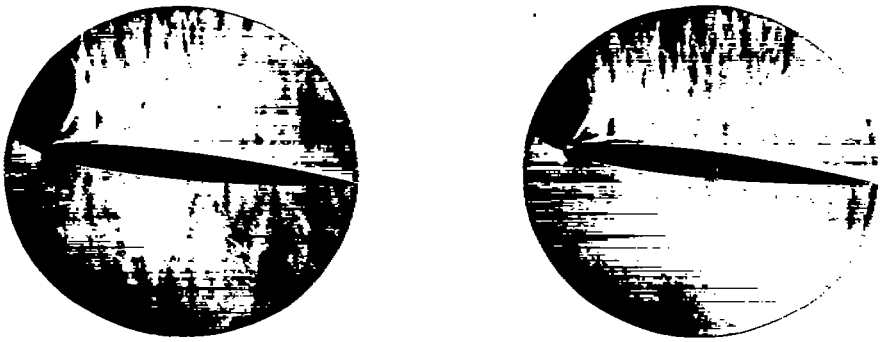

M = 0.65 M = 0.65

M = 0.71 M = 0.71

M = 0.76 M = 0.76

NACA 0009-64 NACA 0009-44

(d) $\alpha = 6^{\circ}$.

NACA L-63561

Figure 13.- Concluded.

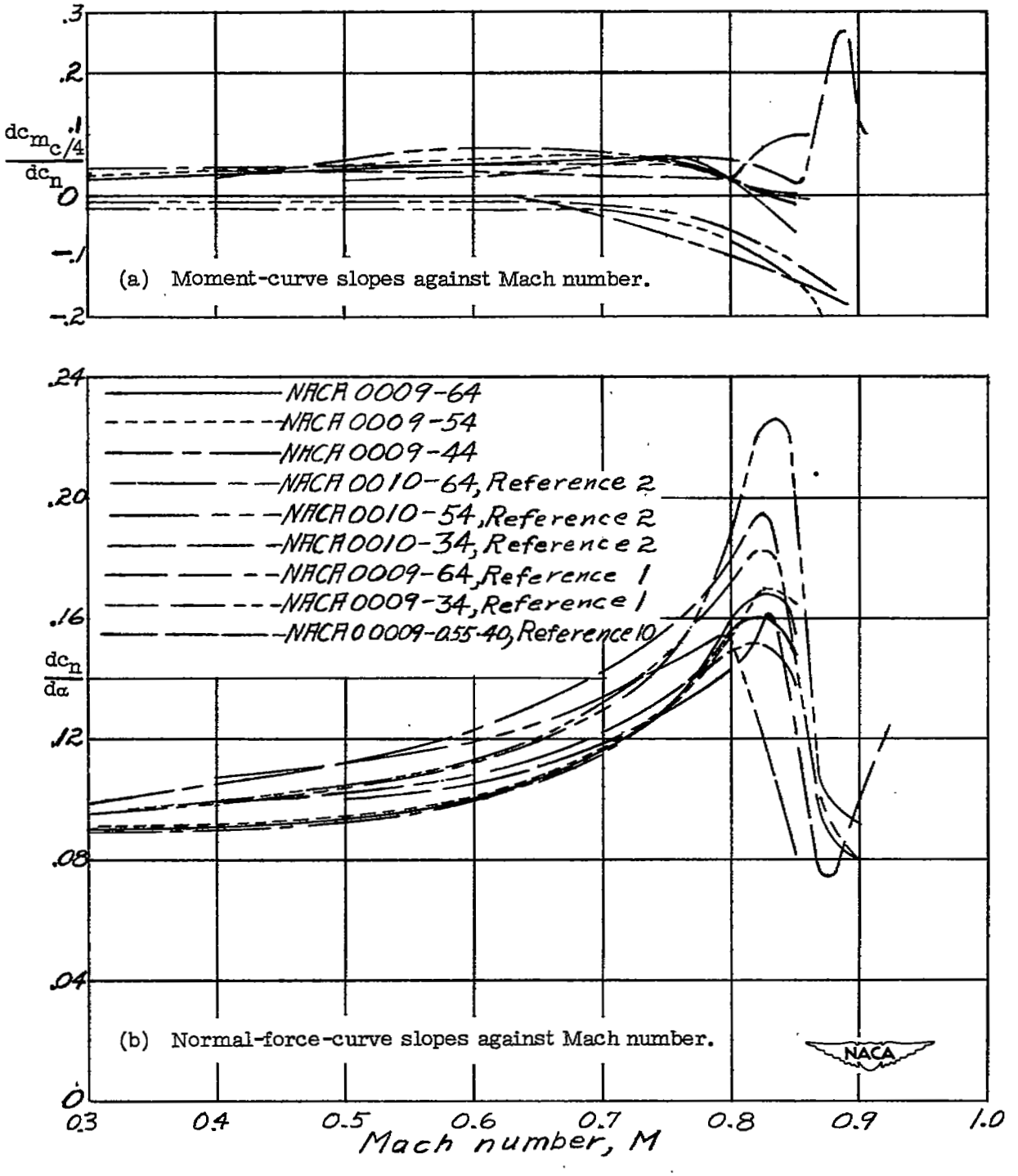

Figure 14.- Comparison of the results with data obtained in other tunnels.

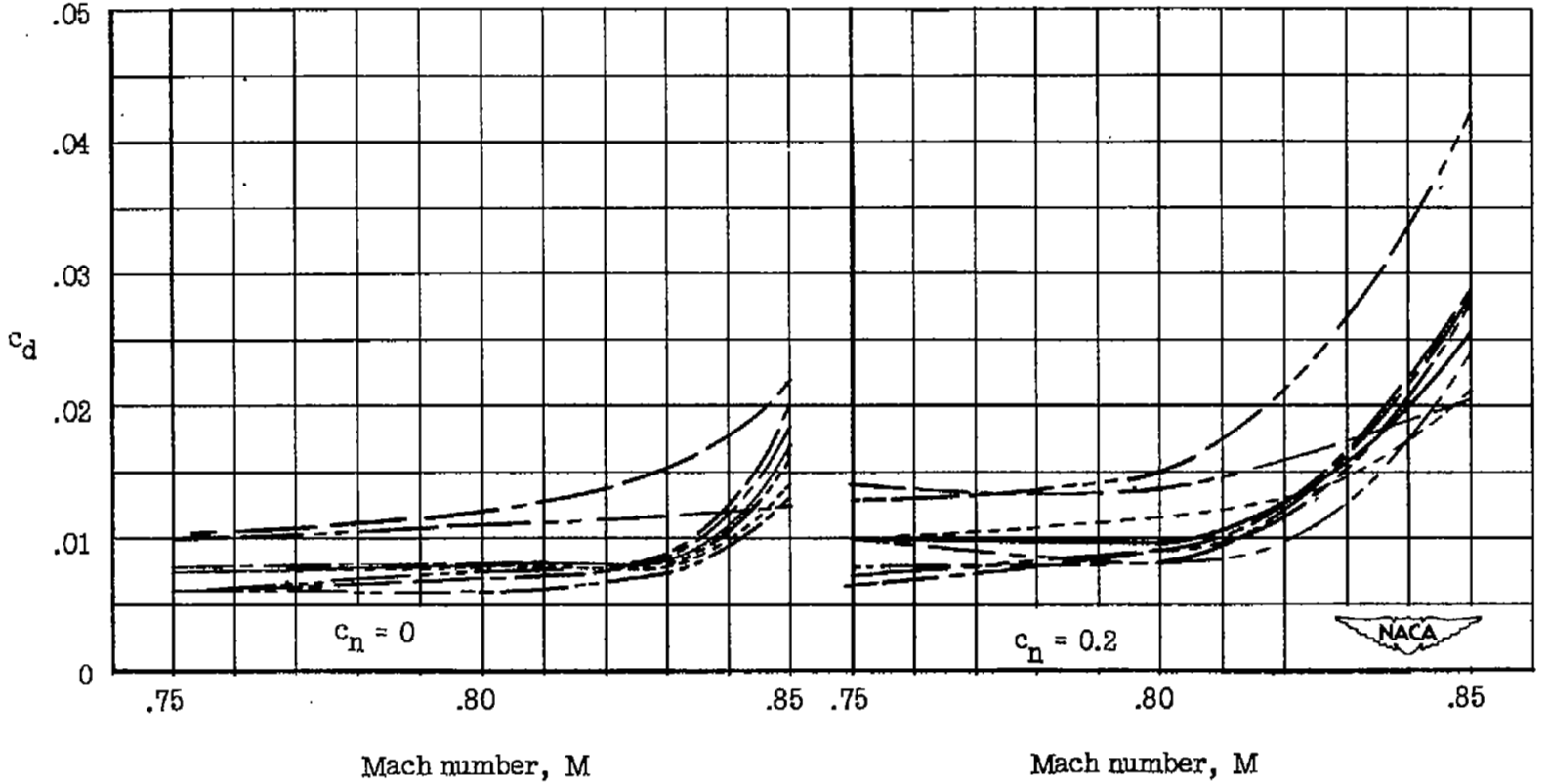

(c) Drag coefficients against Mach number.

Figure 14.- Concluded.